Lithos 196–197 (2014) 181–197

Contents lists available at ScienceDirect

Lithos

journal homepage: www.elsevier.com/locate/lithos

Geochemical fingerprints of Late Triassic calc-alkaline lamprophyres from the Eastern Pontides, NE Turkey: A key to understanding lamprophyre formation in a subduction-related environment

Orhan Karsli [a,*], Abdurrahman Dokuz [b], Melanie Kaliwoda [c], Ibrahim Uysal [d], Faruk Aydin [d], Raif Kandemir [a], Karl-Thomas Fehr [e]

[a] Department of Geological Engineering, Recep Tayyip Erdoğan University, TR-53000 Rize, Turkey
[b] Department of Geological Engineering, Gümüşhane University, TR-29000 Gumushane, Turkey
[c] Mineralogical State Collection Munich, D-80333 München, Germany
[d] Department of Geological Engineering, Karadeniz Technical University, TR-61080 Trabzon, Turkey
[e] Department of Earth and Environmental Sciences, LMU, D-80333 München, Germany

ARTICLE INFO

Article history:
Received 22 November 2013
Accepted 26 February 2014
Available online 6 March 2014

Keywords:
Calc-alkaline lamprophyres
Subcontinental lithospheric mantle
Mantle melting
Late Triassic subduction
Back-arc extension
Eastern Pontides
NE Turkey

ABSTRACT

The Eastern Pontides in NE Turkey is one of the major orogenic belts in Anatolia. In this paper, we report our new $^{40}Ar/^{39}Ar$ dating, mineral chemistry, major and trace elements and Sr–Nd–Pb isotopic analyses of the lamprophyre intrusions in this region. The lamprophyres are widely scattered and intrude Late Carboniferous granitoid rocks. The lamprophyres exhibit fine-grained textures and are mineralogically uniform. Hornblende $^{40}Ar/^{39}Ar$ dating yielded a plateau age of 216.01 ± 10.64 Ma. Based on their geochemistry, mineral compositions and paragenesis, the lamprophyres are classified as calc-alkaline lamprophyres in general and spessartites in particular, which are rich in large ion lithophile elements (e.g., Rb, Ba, K) but depleted in Nb and Ti. Our samples exhibit moderate fractionation in LREE patterns approximately 100 times that of chondrite but HREE abundances less than 10 times that of chondrite. These calc-alkaline lamprophyres display a range of I_{Sr} (216 Ma) values from 0.70619 to 0.71291 and ε_{Nd} (216 Ma) values from −1.4 to 4.1, with T_{DM} = 1.11 to 2.20 Ga. Their Pb isotopic ratios indicate an enriched mantle source. The enrichment process is related to metasomatism of a subcontinental lithospheric mantle source, which is caused by a large quantity of H_2O-rich fluids, rather than sediments released from oceanic crust at depth during the closure of the Paleotethys Ocean in Triassic times. All of the geochemical data and the trace element modeling suggest that the primary magma of the calc-alkaline to high-K calc-alkaline spessartites was generated at depth by a low degree of partial melting (~1–10%) of a previously enriched lithospheric mantle wedge consisting of phlogopite-bearing spinel peridotite. The ascendance of a hot asthenosphere triggered by extensional events caused partial melting of mantle material. The rising melts were accompanied by fractional crystallization and crustal contamination en route to the surface. All of the geochemical features combined with regional data suggest that the Eastern Pontides calc-alkaline lamprophyres originated in an extensional environment along an active continental margin throughout the Late Triassic. Such an extensional event, causing upwelling of hot asthenosphere, led to the opening of the northern branch of the Neotethys as a back-arc basin farther south of the Eastern Pontides.

1. Introduction

The Eastern Pontides, which is the eastern part of the Sakarya Zone, is considered an important natural laboratory for developing an understanding of deep lithospheric processes. Igneous rocks, such as lamprophyres, in this belt record the thermal and geochemical fingerprints of the lithosphere beneath the region. Lamprophyres, a unique type of mesocratic to melanocratic igneous rock with mafic phenocrysts set in a fine-grained matrix, sporadically form as dykes, sills, pipes or small intrusions in various geodynamic settings (Allan and Carmichael, 1984; Duggan and Jaques, 1996; Rock, 1991). These rock types are divided into five primary categories, alkaline lamprophyres, ultramafic lamprophyres, lamproitic lamprophyres, kimberlitic lamprophyres and calc-alkaline lamprophyres (Le Maitre, 1989; Rock, 1991). Calc-alkaline lamprophyres are commonly generated in convergent tectonic settings, whereas alkaline and ultramafic lamprophyres often form in divergent tectonic settings, and kimberlitic lamprophyres are found within plate settings (Carlier et al., 1997). Although lamprophyre outcrops are relatively small, they provide us with new insights into the understanding of large-scale geodynamic processes, in particular continental extension (e.g., Queen et al., 1996; Tappe et al.,

* Corresponding author. Tel.: +90 5322087307; fax: +90 464 2237514.
E-mail address: okarsli@gmail.com (O. Karsli).

http://dx.doi.org/10.1016/j.lithos.2014.02.022
0024-4937/

2006) and mantle enrichment (e.g., Beard et al., 1996; Guo et al., 2004; Srivastava and Chalapathi Rao, 2007). Lamprophyres are considered to be the products of a small degree of partial melting of enriched subcontinental lithospheric mantle sources (e.g., Müller and Groves, 1995; Rock, 1987). Therefore, their geochemical characteristics are closely related to enrichment of the source throughout the evolution of the lithosphere in a dynamic system.

In the study area, very little attention was paid to the calc-alkaline lamprophyre intrusions until recently (Aydin et al., 1997). Here, we present new data, including ^{40}Ar–^{39}Ar hornblende ages, mineral compositions and elemental and Sr–Nd–Pb isotopic compositions of the Late Triassic calc-alkaline lamprophyres from the Eastern Pontides, northeastern Turkey, and we discuss their origin, geodynamic setting and the nature of the lithospheric mantle beneath the region. Particular emphasis is placed on the causes of mantle heterogeneity and the nature of metasomatizing agents in the subcontinental mantle source beneath the Eastern Pontides during the Late Triassic.

2. Regional geology and previous works

Four major tectonic blocks or terranes that are separated by sutures occur in the Anatolia region (e.g., Okay and Tüysüz, 1999). Of these, the Sakarya block is the most important. It represents a series of Mesozoic–Cenozoic fold belts comprising a N-vergent foreland fold thrust belt and a concave, upward-shaped fold belt (Fig. 1a). The eastern part of the Sakarya block is known as the Eastern Pontides, which is a well preserved large mountain belt measuring 500 km long and 100 km wide. The northeast boundary is marked by the Achara-Trialet belt, and the Great Caucausus lies to the north and the Taurides to the south. The basement of the Eastern Pontides consists of Late Carboniferous intrusive and metamorphic rocks; this basement is unconformably overlain by Permo-Carboniferous clastic sedimentary rocks (e.g., Çapkınoğlu, 2003; Dokuz, 2011; Kandemir and Lerosey-Aubril, 2011; Okay and Leven, 1996; Topuz et al., 2007; Topuz et al., 2010; Yilmaz, 1972). Recently, a few upper-mantle serpentinized lherzolite and harzburgite blocks (up to 300 m^2) belonging to the Variscan basement of the Eastern Pontides have been described in the Beyçam (Gümüşhane) and Pulur (Bayburt) areas (Dokuz et al., 2011). The Variscan metamorphic–magmatic basement is unconformably overlain by post Triassic volcano-sedimentary rocks (Dokuz and Tanyolu, 2006; Kandemir and Yilmaz, 2009; Şen, 2007). Late Triassic events in the western part of the Sakarya block are interpreted as associated with a subduction setting, based on the blueschists and eclogites of the Karakaya complex (Okay and Göncüoğlu, 2004; Okay et al., 2002), although this time is poorly understood due to the rarity of the Late Triassic rocks in the Eastern Pontides. The Early Jurassic is dominated by a continental magmatic arc separated from the northern margin of Gondwana in response to the southward subduction of the Paleotethyan oceanic slab during the Early Triassic (Dokuz et al., 2006, 2010; Koçyiğit and Altiner, 2002; Şengör and Yilmaz, 1981; Yilmaz et al., 1997), based on the geochemical nature of the intrusive (Dokuz et al., 2006; Ustaömer and Robertson, 2010) and volcanic rocks (Şen, 2007). This southward subduction of the Paleotethys caused the formation of the northern branch of the Neotethys Ocean in the southern part of the Sakarya Zone (Şengör and Yilmaz, 1981). Middle to Late Jurassic granitoids and dacites emplaced within the volcano-sedimentary rocks of the Şenköy Formation (Dokuz et al., 2006, 2010) together with molasse sediments are interpreted as the products of an arc–continent collision in response to closure of the Paleotethys during the Middle Jurassic and the accretion of the Sakarya block onto Laurasia in the north (Dokuz et al., 2010; Şengör and Yilmaz, 1981; Şengör et al., 1980; Yilmaz et al., 1997). The Late Jurassic to Early Cretaceous was characterized by platform carbonates of the Berdiga Formation (Görür, 1997; Tüysüz, 1999). During the Late Cretaceous, the opening of the Black Sea in the northern part of the Eastern Pontides was triggered by the northward subduction of the Neotethys (Okay et al., 1994; Robinson et al., 1995; Şengör et al., 2003). This subduction resulted in a submarine magmatic arc (Altherr et al., 2008; Boztuğ and Harlavan, 2008; Boztuğ et al., 2004; Çinku et al., 2010; Karsli et al., 2010a, 2012a; Kaygusuz et al., 2008; Okay and Şahintürk, 1997; Okay and Tüysüz, 1999; Ustaömer and Robertson, 2010; Yilmaz et al., 1997). The Early Paleocene plagioleucitites in the Eastern Pontides have been interpreted as the final products of the northward subduction (Altherr et al., 2008). The Paleocene and Early Eocene in the Eastern Pontides were dominated by continent–continent collision between the Pontides and the Tauride–Anatolide block in response to the complete closure of the Neotethys (Boztuğ et al., 2004; Dokuz et al., 2013; Hisarli, 2011; Karsli et al., 2010b, 2011; Okay and Şahintürk, 1997; Rolland et al., 2012; Topuz et al., 2011). Middle Eocene high-K calc-alkaline intrusives and volcanics (Arslan and Aslan, 2006; Aydinçakir and Şen, 2013; Boztuğ et al., 2004, 2006; Karsli et al., 2007, 2012b) and Neogene alkaline volcanics (Aydin et al., 2008, 2009) formed in a post-collision extensional setting.

3. Sampling and analytical techniques

We collected fourteen lamprophyre samples at three locations of small intrusions near the village of Karamustafa, Gümüşhane (Fig. 1b). The sample locations are depicted in Fig. 1b. All of the samples are megascopically fresh, undeformed and unmetamorphosed. As these samples represent the first observation of such rocks in the region, $^{40}Ar/^{39}Ar$ dating, mineral chemical analyses, major and trace element analyses, and Sr–Nd–Pb isotopic measurements were performed to evaluate the origin of the calc-alkaline lamprophyres in the Eastern Pontides and the geodynamic setting in which they were generated.

3.1. $^{40}Ar/^{39}Ar$ dating

$^{40}Ar/^{39}Ar$ incremental heating experiments were performed in the Geochronology Laboratory at the Vrije University. For each sample, approximately 200 mg of washed groundmass was packed in 20-mm diameter Al-foil packages and was stacked with packages containing a mineral standard into a 23-mm OD quartz tube. The mineral standard was DRA-1 sanidine (with a K/Ar age of 25.26 Ma), and the quartz vial was packaged in a standard Al-irradiation capsule and irradiated for 1 h in a Cd-lined rotating apparatus at the NRG-Petten HFR facility in the Netherlands. Laser incremental heating was performed using a Synrad 48-5 CO_2 laser. A typical mass spectrometer run consisted of stepping through the argon mass spectrum. The details of the analytical method were those described by Wijbrans et al. (1995).

3.2. Microchemical analyses

The mineral compositions were determined in polished thin sections using a Cameca SX-100 electron microprobe at the Ludwig Maximilian University, Section for Mineralogy, Petrology and Geochemistry, Munich (Germany), equipped with five wavelength-dispersive spectrometers. The analytical conditions included an accelerating voltage of 15 kV, a beam current of 20 nA and a counting time of 10 to 30 s.

Fig. 1. (a) Main tectonic setting of Turkey in relation to the Afro-Arabian and Eurasian plates [modified from Okay and Tüysüz (1999)]. (b) Simplified geological map of the Gümüşhane area and (c) Detailed geological map of the Karamustafa area containing the calc-alkaline lamprophyres. Localities: KLM1 = 40°21′32″N, 39°19′26″E; KML10 = 40°21′10″N, 39°18′20″E; KML15 = 40°20′33″N, 39°18′33″E.

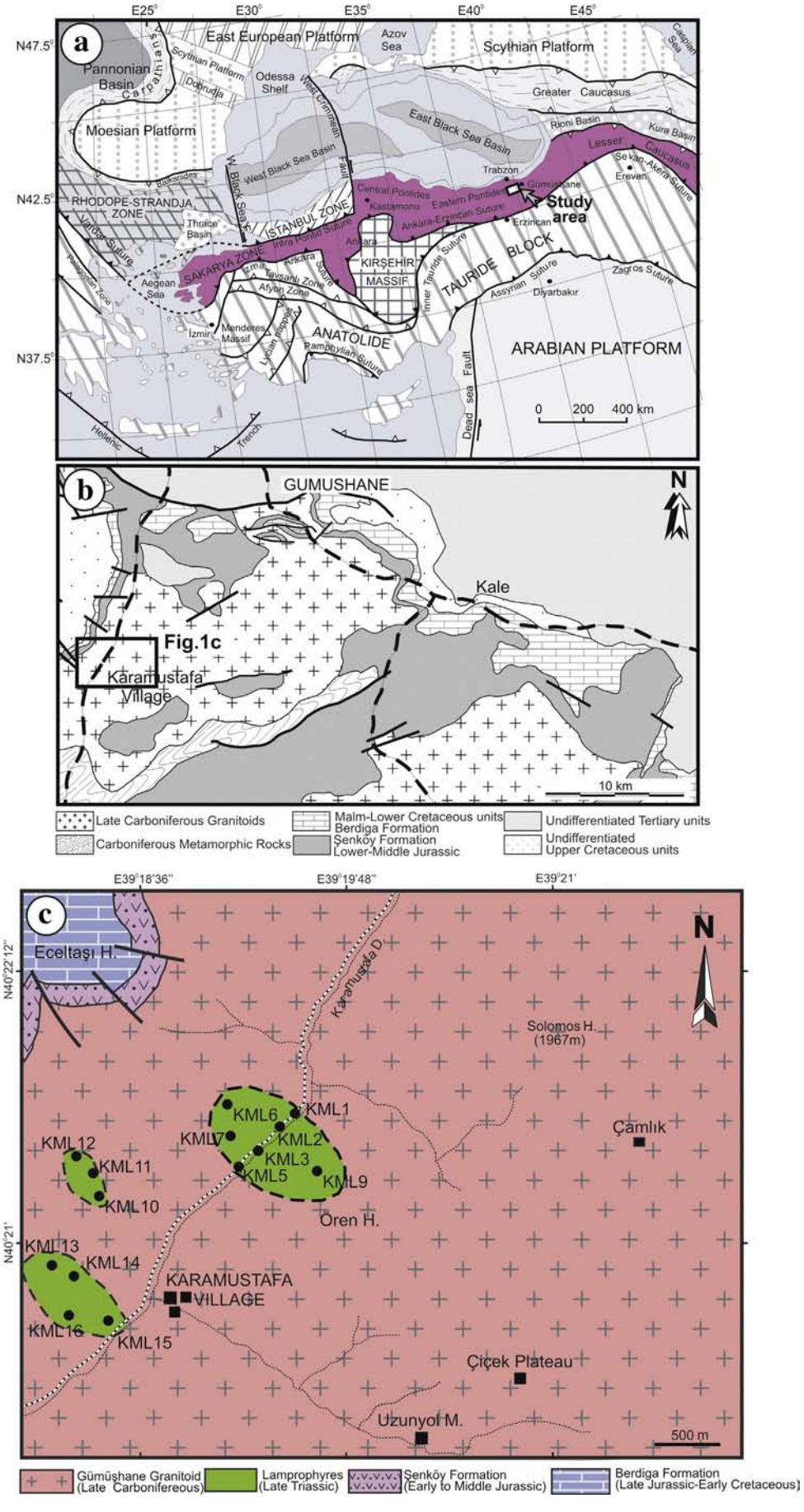
a
East European Platform
Azov Sea
Scythian Platform
Caspian Sea
Pannonian Basin
Carpathians
Scythian Platform
Dobrudja
Odessa Shelf
West Crimmerian Fault
Greater Caucasus
Moesian Platform
East Black Sea Basin
Rioni Basin
Kura Basin
Lesser Caucasus
West Black Sea Basin
W. Black Sea Fault
Balkanides
Trabzon
Sevan-Akera Suture
Erevan
RHODOPE-STRANDJA ZONE
Central Pontides
Eastern Pontides
Gumushane
Study area
Kastamonu
Ankara-Erzincan Suture
Thrace Basin
ISTANBUL ZONE
Intra Pontid Suture
Erzincan
Ankara
Izmir-Ankara Suture
SAKARYA ZONE
KIRŞEHIR MASSIF
TAURIDE BLOCK
Inner Tauride Suture
Aegean Sea
Tavsanli Zone
Afyon Zone
Assyrian Suture
Zagros Suture
Diyarbakır
Menderes Massif
ANATOLIDE
Lycian Nappes
Pamphylian Suture
ARABIAN PLATFORM
Dead sea Fault
Hellenic Trench
0 200 400 km
N47.5°
N42.5°
N37.5°
E25°
E30°
E35°
E40°
E45°
b
GUMUSHANE
N
Kale
Fig.1c
Karamustafa Village
10 km
Late Carboniferous Granitoids
Carboniferous Metamorphic Rocks
Malm-Lower Cretaceous units Berdiga Formation
Senköy Formation Lower-Middle Jurassic
Undifferentiated Tertiary units
Undifferentiated Upper Cretaceous units
c
E39°18'36"
E39°19'48"
E39°21'
N40°22'12"
N40°21'
Eceltaşı H.
Karamustafa D.
Solomos H. (1967m)
Çamlık
KML1
KML2
KML3
KML5
KML6
KML7
KML9
KML10
KML11
KML12
KML13
KML14
KML15
KML16
Ören H.
KARAMUSTAFA VILLAGE
Çiçek Plateau
Uzunyol M.
500 m
Gümüşhane Granitoid (Late Carboniferous)
Lamprophyres (Late Triassic)
Senköy Formation (Early to Middle Jurassic)
Berdiga Formation (Late Jurassic-Early Cretaceous)

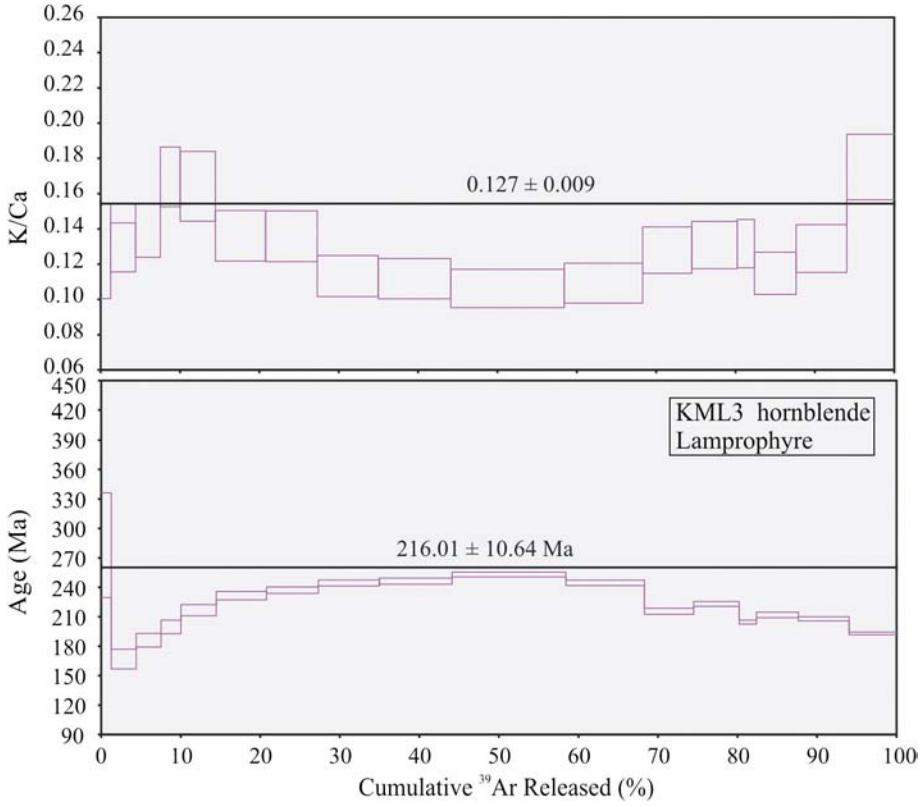

Fig. 2. $^{40}Ar/^{39}Ar$ age and K/Ca spectra plots of the hornblende from the calc-alkaline lamprophyre intrusion by incremental heating.

Synthetic and natural oxides and silicates were used as standard materials. The correction procedures were based on the CAMECA PAP algorithm by Pouchou and Pichoir (1985). The detection limits were generally in the order of 0.1 wt.%. The counting time was usually set to 10 s when analyzing for the major elements (i.e., Si, Al, Fe, Ca, Na and K). The analyses were performed using a beam diameter of 1 μm, except in the case of feldspars, in which a defocused beam (10 μm) was used to minimize the alkaline diffusion.

3.3. Whole-rock major and trace element analyses

Twelve samples were selected for the major and trace element analyses. To prepare the rock powders, 1–3 kg of each sample was crushed in a steel crusher, and the samples were then crushed further in an agate mill to a grain size of <200 mesh. The major and trace element concentrations were determined at the commercial ACME Laboratories Ltd, in Vancouver, Canada. The amounts of major element oxides were measured using ICP-AES (0.2 g of pulp sample by $LiBO_2$ fusion). The detection limits are approximately 0.001–0.04%. For the trace element analyses, 0.2 g of sample powder and 1.5 g of $LiBO_2$ flux were mixed in a graphite crucible and heated to 1050 °C for 15 min in a muffle furnace. The molten sample was then dissolved in 100 mL of 5% HNO_3 (American Chemical Society-grade nitric acid in deionized water). The sample solutions were shaken for 2 h, and then an aliquot was poured into a polypropylene test tube and aspirated into a Perkin-Elmer Elan 600 ICP mass spectrometer. Calibration and verification standards together with reagent blanks were added to the sample sequence. The elemental concentrations of the samples were obtained using BCR-2 and BIR-2 (concentrations from USGS) as external standards. The detection limits ranged from 0.01 to 0.5 ppm for most of the trace elements.

3.4. Sr–Nd–Pb isotopic analyses

Powdered samples were dissolved using acid ($HF + HClO_4$) in sealed Savillex beakers on a hot plate for one week. Sr and Nd isotopic analyses were performed at the Institute of Geology and Geophysics, Chinese Academy of Sciences (Beijing). Isotope analyses were performed using a multi-collector VG354 mass spectrometer. Rb, Sr, Sm and Nd concentrations were measured using the isotopic dilution method. $^{87}Sr/^{86}Sr$ ratios

Table 1
$^{40}Ar/^{39}Ar$ age data of the calc-alkaline lamprophyres from the Gümüşhane region in the Eastern Pontides.

Sample	Rock type	Mineral	Plateau age		Normal isochron					
			Age ± 2σ (Ma)	MSWD	Age ± 2σ (Ma)	$^{40}Ar/^{36}Ar(i)$ ± 2σ	MSWD	$^{39}Ar_{(K)}$ %	(n)	K/Ca ± 2σ
KML3	Calc-alkaline lamprophyre	Hornblende	216.01 ± 10.64	242.75	200.02 ± 19.60	309.22 ± 18.15	100.10	100.01	17	0.127 ± 0.01

Note: Plateaus ages were calculated over concordant steps (as defined by the MSWD value calculated for the plateau steps), the percentage of the gas release included in the plateau calculation is given in the column $^{39}Ar_{(K)}$, the number of steps forming the plateau is n. 40/36(i) refers to the non-radiogenic intercept ratio of $^{40}Ar/^{36}Ar$, which are in all cases indistinguishable from the value for modern air. Isochron ages were calculated over the steps that represent the plateau. Errors given are ±2σ. Ages were calculated on the basis of an age for the laboratory standard sanidine DRA-1 of 25.26 ± 0.2 Ma.

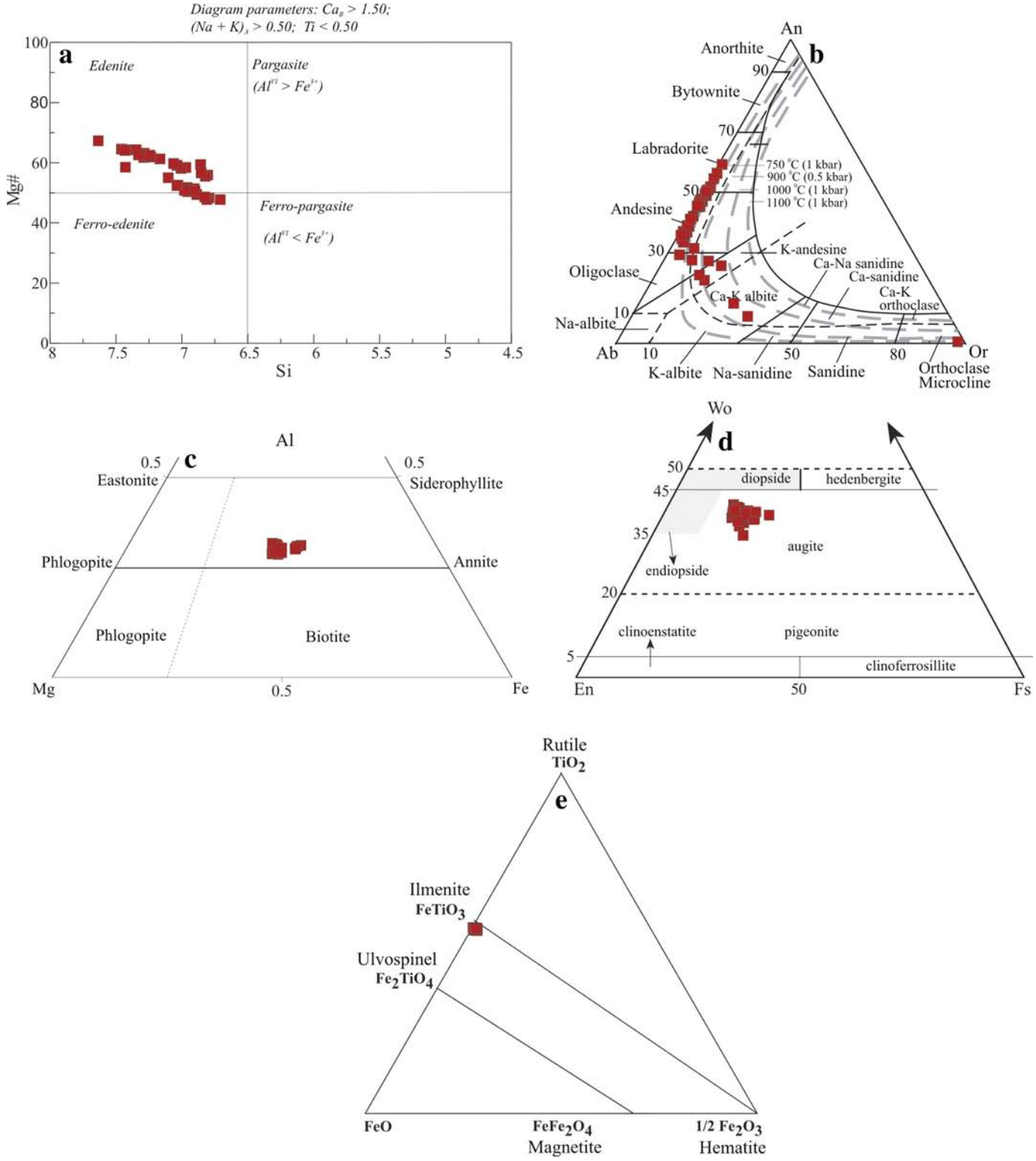

Fig. 3. (a) Nomenclature of the amphiboles from the calc-alkaline lamprophyres. (b) Portion of the feldspar ternary diagram showing the feldspar composition. (c) Nomenclature of the biotites from the studied samples. (d) The pyroxene composition shown on the enstatite–diopside half of the pyroxene quadrilateral. (e) The ilmenite compositions represented as molar proportions in the $FeO–Fe_2O_3–TiO_2$ ternary.

were normalized against $^{86}Sr/^{88}Sr = 0.1194$, and $^{143}Nd/^{144}Nd$ ratios were normalized against $^{146}Nd/^{144}Nd = 0.7219$. $^{87}Sr/^{86}Sr$ ratios were adjusted to the NBS-987 Sr standard = 0.710250 and $^{143}Nd/^{144}Nd$ ratios to the La Jolla Nd standard = 0.511860. The uncertainty in concentration analyses by isotopic dilution is ±2% for Rb, ±0.4–1% for Sr, and <±0.5% for Sm and Nd, depending on concentration levels; with an overall uncertainty for Rb/Sr is ±2% and for Sm/Nd is ±0.2–0.5%. Procedural blanks are: Rb = 120 pg, Sr = 200 pg, Sm = 50 pg and Nd = 50–

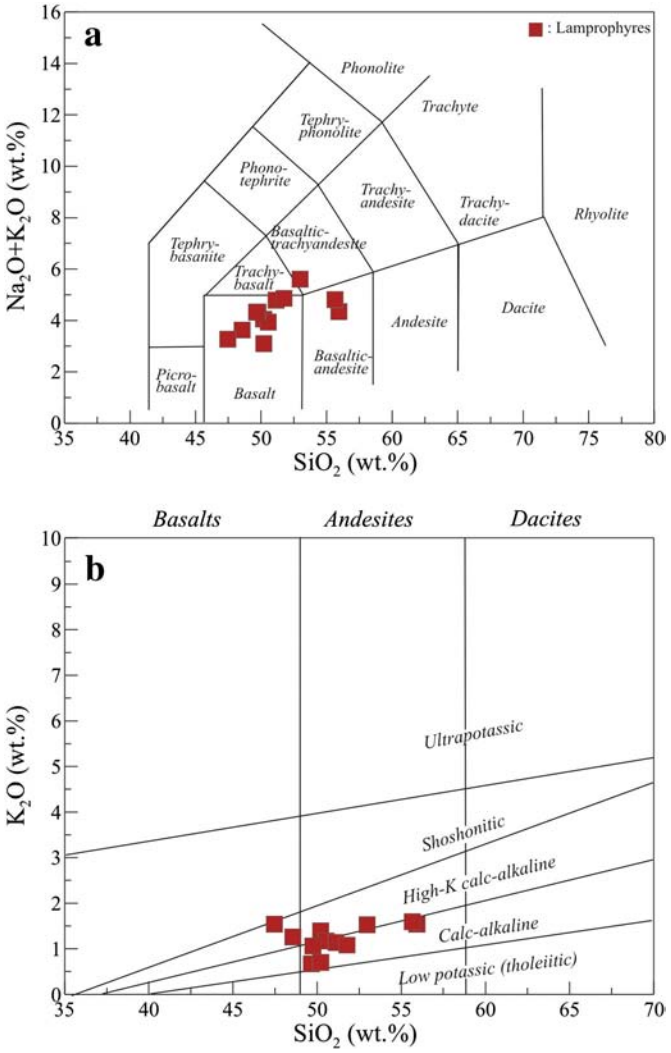

Fig. 4. Classifications of the calc-alkaline lamprophyres from the Gümüşhane region. (a) The TAS diagram (Le Bas et al., 1986), (b) K_2O–SiO_2 diagram (Peccerillo and Taylor, 1976) for the lamprophyres.

100 pg. The detailed analytical procedures for Sr and Nd isotopic measurements are given in Qiao (1988), and for the analysis of Pb isotope, the sample powder was spiked and dissolved in concentrated HF at 800 °C for 72 h. Lead was separated and purified by a conventional anion-exchange technique (AG1×8, 200–400 resin) with diluted HBr. Isotopic ratios were measured using the VG-354 mass spectrometer at the IGG (Beijing). Repeated analyses of NBS981 resulted in $^{204}Pb/^{206}Pb = 0.05897 \pm 15$, $^{207}Pb/^{206}Pb = 0.91445 \pm 80$ and $^{208}Pb/^{206}Pb = 2.16170 \pm 200$.

4. Results

4.1. $^{40}Ar/^{39}Ar$ dating

The $^{40}Ar/^{39}Ar$ incremental heating method was used for the dating of the lamprophyres. The resulting $^{40}Ar/^{39}Ar$ data are presented in Table 1 and Fig. 3, representing the results in the form of age spectra. The $^{40}Ar/^{39}Ar$ dating of a hornblende separate from the spessartites (sample KML3) yielded a plateau age of 216 ± 10.64 Ma. The plateau is defined by seventeen steps. The hornblende separate produced the best results, with reasonable enrichment in radiogenic argon and good agreement between the plateau and isochron ages (Table 1). The alignment of points in the isochron plots seems to indicate that there is extraneous (perhaps inherited or excess) ^{40}Ar in the system. The plateau age of 216 ± 10.64 Ma of the hornblende separate from the lamprophyres is thought to date the crystallization time of the lamprophyres, coinciding with the subduction events in the region (Dokuz, 2011; Okay and Tüysüz, 1999; Şengör and Yilmaz, 1981; Yilmaz et al., 1997). (See Fig. 2.)

4.2. Mineralogy and petrography

Based on the mineral paragenesis and geochemical compositions, the mafic rocks collected from the Karamustafa area, Gümüşhane, are classified as lamprophyres, and none of the samples resemble a lamproite. The lamprophyres are present as small intrusions within the Late Carboniferous intrusive rocks of the Gümüşhane granitoid. The individual stocks are <2 km in diameter (Fig. 1b). Most of the lamprophyres are fresh. On the basis of their silicate mineralogy, the rocks are spessartites. All of the samples display porphyritic textures typical of lamprophyres, with variably sized phenocrysts of plagioclase, calcic amphibole ± biotite and pyroxene set in a groundmass of plagioclase and amphibole ± K-feldspar with such accessory minerals as ilmenite and apatite. The groundmass is typically holocrystalline, with a fine grained nonequigranular texture. No glass has been found. Glomeroporphyritic clusters of amphibole and plagioclase are present. The amphibole and plagioclase phenocrysts are typically less than 2 mm in diameter but may comprise up to 40% of the samples. The amphibole phenocrysts are of homogeneous composition, with X_{Mg} [= Mg / (Mg + Fe_{tot})] ranging from 0.48 to 0.68, clustering in the edenite and ferro-edenite fields, according to Leake et al. (1997), in contrast to the K-rich amphiboles typical of lamproites (Fig. 3a; Supplementary Table 1). The compositions of the matrix amphiboles overlap with those of the phenocrysts. The plagioclase phenocrysts are subhedral and are found together with microlites of mafic silicates. The spessartites contain plagioclase phenocrysts (from andesine to labradorite) with a composition of $Ab_{63-40}An_{59-31}Or_{7-1}$ (Fig. 3b; Supplementary Table 1). The compositions of all of the phenocrysts are similar to those of the minerals in the groundmass. A minority of the alkali feldspars in the groundmass are orthoclase of entirely homogeneous composition (Or_{99-100}) (Fig. 3b). The lesser amounts of subhedral biotite and pyroxene fit the modal definition of spessartites. Highly pleochroic biotites from the spessartites contain variable amounts of TiO_2 (2.60–4.68 wt.%) and have X_{Mg} values of 0.44 to 0.53 (Fig. 3c; Supplementary Table 1). Clinopyroxene is present as small subhedral grains (~1 mm). Based on the criteria of Morimoto et al. (1988), the clinopyroxenes are of augite composition, i.e., $Wo_{36-45}En_{36-47}Fs_{11-22}$ (Fig. 3d). The augitic pyroxenes have X_{Mg} values ranging from 0.73 to 0.77. Ilmenites are present as poikilitic inclusions within mafic silicates and are of homogeneous composition ($Ilm_{99}Hm_{01}$) (Fig. 3e; Supplementary Table 1).

4.3. Major and trace elements

In the total alkali–silica diagram (Fig. 4a), the lamprophyres fall in the fields of basalt, basaltic–andesite and basaltic trachyandesite, having low to moderate SiO_2 contents (Table 2). The Mg# [(100 × MgO / (MgO + 0.9FeO_{tot})] varies widely, ranging from 47 to 73, due to the magma evolution. All of the samples lie within the high-K calc-alkaline and calc-alkaline fields defined by Peccerillo and Taylor (1976) (Fig. 4b). The concentrations of transition metals (Table 2) in the lamprophyres are lower than those of primitive mafic magmas (Frey et al., 1978), suggesting the more differentiated nature of the former. Diagrams of the major and trace elements versus silica shown in Fig. 5a–g display linear and scattered trends. It is apparent that all of the rocks generally exhibit negative correlations between SiO_2 and MgO and CaO, respectively, while they have a positive correlation between silica and Na_2O (Fig. 5).

In the diagrams of multiple-element variations (Fig. 6a), all of the samples exhibit similar patterns, specifically significant enrichment in

Table 2
Representative whole-rock analyses for major and trace elements of the calc-alkaline lamprophyres from the Eastern Pontides.

Rock type	Calc-alkaline lamprophyres											
Sample no	KML1	KML2	KML3	KML5	KML6	KML7	KML9	KML10	KML11	KML12	KML15	KML16
SiO_2	52.98	50.2	50.54	49.75	49.66	51.13	51.76	48.55	47.47	50.21	55.93	55.65
TiO_2	0.86	1.08	1.13	1.71	1.26	1.68	0.75	0.97	0.71	0.54	0.71	0.71
Al_2O_3	16.2	14.84	14.69	15.07	14.47	15.31	16.49	15.92	16.51	14.4	16.83	17.22
$Fe_2O_3^t$	7.93	10.85	10.17	11.01	11.8	10.61	7.5	9.36	10.27	8	8.02	8.17
MnO	0.13	0.19	0.21	0.22	0.19	0.18	0.14	0.16	0.17	0.14	0.16	0.16
MgO	6.83	7.67	8.2	6.86	7.03	5.94	7.74	8.9	9.87	10.64	3.78	3.63
CaO	7.77	9.48	9.77	9.33	8.72	8.68	8.62	9.82	8.62	10.18	6.94	7.17
Na_2O	4.08	2.66	2.77	3.27	3.65	3.65	3.78	2.37	1.73	2.4	2.81	3.22
K_2O	1.53	1.39	1.17	1.06	0.67	1.14	1.08	1.26	1.54	0.7	1.54	1.59
P_2O_5	0.108	0.118	0.09	0.13	0.12	0.15	0.08	0.09	0.06	0.06	0.15	0.16
LOI	1.3	1.3	1.1	1.1	2.3	1.4	1.9	2.3	2.7	2.4	2.9	2.1
Total	99.71	99.77	99.84	99.6	99.8	99.87	99.84	99.70	99.65	99.67	99.77	99.78
Mg#	0.63	0.58	0.62	0.55	0.53	0.53	0.67	0.65	0.66	0.73	0.48	0.47
Rb	64.3	51.7	40.6	26.1	19.8	44.4	44.3	47.5	69.2	25.3	38.2	43.4
Sr	146.5	269	164.6	198.2	176.8	207.2	309.9	299	216.7	259.5	313.5	372.2
Ba	248	159	135.4	258.4	81.1	136.9	148	217	393	143	498	470
Cs	1.9	1.6	1.4	1	0.8	2	1.1	2.6	2.7	1.7	1.4	1.6
Zr	71.2	75	69.6	97.3	83.2	123.2	63.1	66.8	44.1	40.4	121.1	112.4
Hf	2.5	2.1	1.9	2.8	2.3	3.5	2	2	1.4	1.1	3.2	3.3
Th	2.7	2.3	3	2.4	1.8	2.9	3	1.3	1.7	3.4	6.2	5.7
Pb	2.2	7	9.2	5	1.8	8.8	6.6	4.6	5.7	4.5	6.9	8
Nb	2.2	3	2.3	3	2.6	3.7	2.2	1.6	1.2	1	6.2	6
Y	18.8	19.6	25.9	26.6	34.4	19	20.2	21.5	20.6	11.7	22.3	22.1
Ni	29.8	6.4	24.5	9.3	13	8	29.9	44	79	72.4	7.2	5.7
Co	32.3	40.8	42.6	38.9	43	36.5	35.3	42.2	47.6	46.8	21.1	21.4
V	176	221	242	380	258	311	182	240	188	203	194	193
Ta	0.2	0.2	0.2	0.2	0.2	0.3	0.1	0.1	0.1	0.1	0.4	0.4
La	8.2	6	5.6	6.7	5.6	8.6	7.4	4.4	4.4	4.2	20.2	19.1
Ce	15.5	12.2	13.9	17.4	13.8	21.6	17	10.6	9.8	8.8	40.8	38.6
Pr	2.37	2.13	1.9	2.46	2.04	3.03	2.09	1.57	1.34	1.17	4.66	4.49
Nd	10.3	10.1	9.5	12	9.1	14	9.1	7.7	6.6	5.1	19	18.1
Sm	2.84	2.89	2.97	3.56	2.92	4.3	2.43	2.28	1.89	1.46	3.83	3.68
Eu	0.74	0.89	0.77	1.13	0.94	1.29	0.7	0.99	0.68	0.53	1.07	1.04
Gd	3.32	3.5	3.65	4.5	3.79	5.12	2.81	2.97	2.67	1.78	3.74	3.63
Tb	0.53	0.54	0.7	0.83	0.71	0.96	0.52	0.58	0.53	0.33	0.64	0.61
Dy	3.88	3.88	3.91	4.68	4.14	5.45	3.06	3.53	3.29	1.9	3.69	3.49
Ho	0.76	0.82	0.83	0.96	0.89	1.13	0.62	0.76	0.71	0.41	0.78	0.74
Er	2.24	2.27	2.47	2.69	2.52	3.22	1.75	2.14	2.15	1.18	2.22	2.18
Tm	0.34	0.35	0.36	0.42	0.39	0.48	0.28	0.34	0.32	0.18	0.36	0.34
Yb	2.15	2.33	2.42	2.71	2.67	3.17	1.72	2.12	2.13	1.07	2.28	2.22
Lu	0.35	0.35	0.36	0.37	0.37	0.43	0.24	0.32	0.32	0.17	0.35	0.34
(La/Yb)cn	2.57	1.74	1.56	1.67	1.41	1.83	2.90	1.40	1.39	2.65	5.97	5.80
Eu/Eu*	0.73	0.85	0.71	0.86	0.86	0.83	0.81	1.16	0.92	1.00	0.86	0.86

Note: Mg# is 100 × MgO / (MgO + 0.9FeO_{tot}) in molar proportions. Oxides are given in wt.%, trace elements in μg/g.

large-ion lithophile elements (LILEs) (Ba, Rb, Th and K) relative to certain high field-strength elements (HFSEs) (such as Nb and Ti), with negative Nb anomalies. The patterns of the chondrite-normalized rare earth elements (REEs) display enrichment in LREEs relative to HREEs (Fig. 6b), with negligible negative Eu anomalies (Eu/Eu* = 0.71 to 1.16; Table 2). The value of (La/Yb)cn is low to moderate, between 1 and 5, with mostly low values of <2 (Table 2).

4.4. Lamprophyre signature

The term 'lamprophyre', with hypabyssal and mesocratic to melanocratic characteristics, was first reported by Gumbel Von (1874) in classifying quartz-free, volatile-rich, sodic to potassic and mafic–ultramafic alkaline igneous rocks. The lamprophyres were later divided into five primary categories: calc-alkaline lamprophyres, alkaline lamprophyres, ultramafic lamprophyres, lamproitic lamprophyres and kimberlitic lamprophyres (Rock, 1987, 1991). The samples analyzed in our study fall within the field of calc-alkaline lamprophyres in the classification diagram (Fig. 7a). Likewise, their mafic silicate compositions (i.e., amphibole, biotite and pyroxene) suggest that they plot in the calc-alkaline lamprophyre fields of the selected classification diagrams (Fig. 7b–d).

4.5. Sr–Nd–Pb isotopes

Measured and Sr–Nd–Pb isotope data for five representative samples from the calc-alkaline lamprophyres from the Karamustafa area, Gümüşhane, are presented in Tables 3 and 4. The lamprophyres display relatively high and heterogeneous isotopic compositions: their I_{Sr} (216 Ma) ranges from 0.70619 to 0.71291, and their ε_{Nd} (216 Ma) ranges from −1.4 to 4.1. The corresponding Nd model ages (T_{DM}) are in the range of 1.56 to 2.20 Ga. All of the samples exhibit a slight negative correlation between the two parameters; in other words, ε_{Nd} (216 Ma) decreases with increasing I_{Sr} values. The lamprophyre samples plot primarily in the right quadrants of the conventional Sr–Nd isotope diagram. Compared with volcanics and other granitoids of Late Cretaceous to Early Cenozoic ages from the Eastern Pontides, they have Sr–Nd isotopic values different from those of the lower crust-derived, Early Cenozoic adakitic volcanics (Karsli et al., 2010b) and granitoids (Topuz et al., 2005), the Neogene alkaline volcanics (Aydin et al., 2008), hybrid granitoids from the Eastern Pontides (Karsli et al., 2007), the subduction-related plagioleucitites (Altherr et al., 2008), Late Cretaceous hybrid Harşit pluton (Karsli et al., 2010a), A-type granites from the Eastern Pontides (Karsli et al., 2012a) and Middle Eocene shoshonitic granitoids (Karsli et al., 2012b) (Fig. 8a).

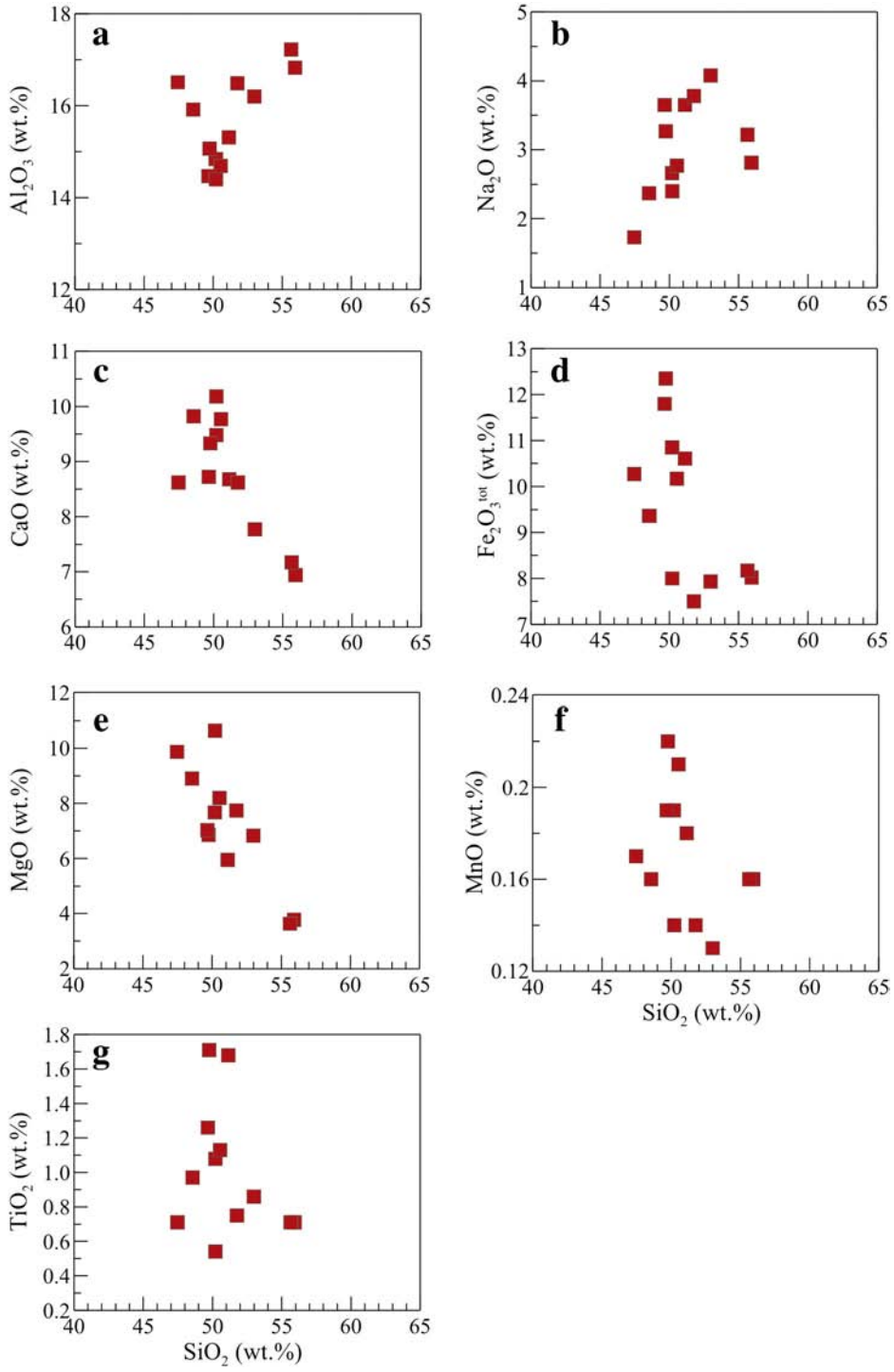

Fig. 5. Harker plots of the calc-alkaline lamprophyres. (a) SiO_2 versus Al_2O_3; (b) SiO_2 versus Na_2O; (c) SiO_2 versus CaO; (d) SiO_2 versus $Fe_2O_3^{tot}$ (e) SiO_2 versus MgO; (f) SiO_2 versus MnO; (g) SiO_2 versus TiO_2.

The lamprophyre samples are relatively homogeneous in their lead isotopic compositions, specifically their $^{206}Pb/^{204}Pb$, $^{207}Pb/^{204}Pb$ and $^{208}Pb/^{204}Pb$ isotopic ratios. The lead isotopic ratios of the samples are radiogenic (Fig. 8b, c and Table 4). The northern hemisphere reference line (NHRL; Hart, 1984) was used in the plots, as the ^{208}Pb data are more radiogenic than the ^{206}Pb that plot well above the NHRL in conventional Pb isotope diagrams (Fig. 8a, b). The EM1 and EM2 end-members (Zindler and Hart, 1986) are also plotted for comparison. The field of the Sisdağı pluton is shown for reference, and the Pb isotopes of the samples are clustered in a field near the fields of the Sisdağı pluton and marine sediments, far from that of EM1, and tending toward that of the EM2 end-member (Fig. 8a, b).

5. Discussion

5.1. Petrogenesis of the calc-alkaline lamprophyre intrusions

The calc-alkaline lamprophyres investigated in the region are scattered, and their distribution, petrography, mineralogy and geochemistry differ greatly from those of the other rock. Their

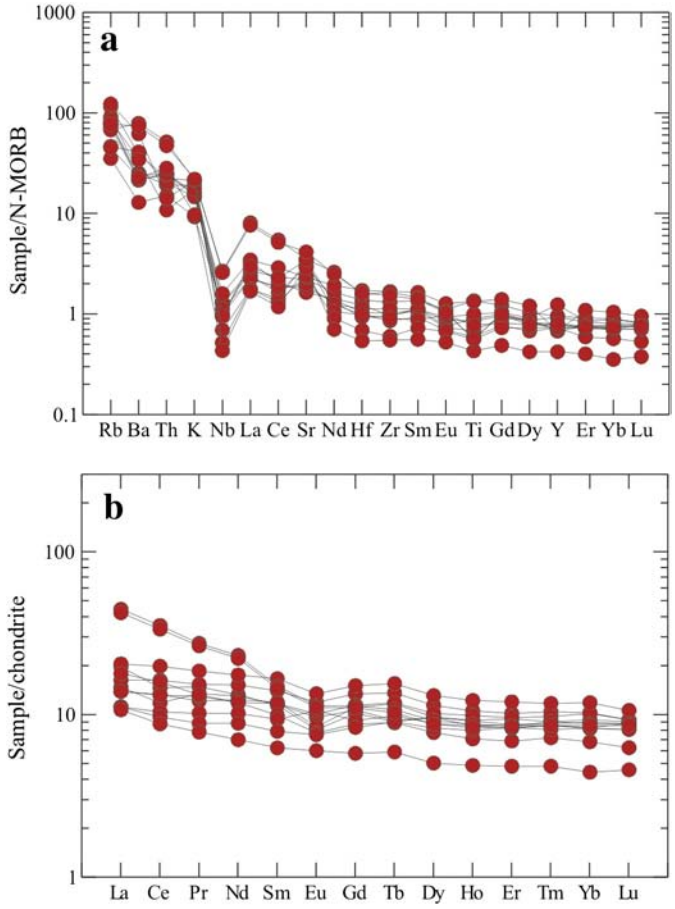

Fig. 6. (a) N-MORB-normalized multi-element variation patterns (normalized to values given in Sun and McDonough, 1989) for the calc-alkaline lamprophyres. (b) Chondrite normalized (to values given in Boynton, 1984) rare earth element abundance patterns for the selected samples from the lamprophyre intrusion.

calc-alkaline character is clearly indicated by their major element concentrations and mineral compositions. The negative Nb and Ti spikes in the N-MORB normalized multi-element diagrams are indicative of subduction-related melts or melts derived from melting of a mantle wedge that was enriched by previous subduction events in a post-orogenic setting. Thus, the calc-alkaline lamprophyres may be products of a basic parental magma evolved by fractional crystallization (e.g., Currie and Williams, 1993) or a mantle source modified by subduction-related fluids (e.g., Awdankiewicz, 2007; Nédli and Tóth, 2007; Prelevic et al., 2005). All of the results presented here support the scenario of melts formed in an extensional environment of a subduction setting. The principal lines of evidence for this possibility are discussed in detail below.

5.1.1. Magma evolution

The negative correlation in the plots of MgO–SiO_2 and CaO–SiO_2 suggests the fractionation of the ferromagnesian minerals during magma evolution. In addition, there are no correlations in the plots of $Fe_2O_3^{tot}$–SiO_2 and TiO_2–SiO_2, clearly indicating that rutile and Fe–Ti oxide fractionation was not responsible for the evolution of the parental magma of the lamprophyres (Fig. 5a–g). Small amounts of plagioclase fractionation are supported by the weak Eu/Eu* anomalies and negative CaO–SiO_2 correlations. The I_{Sr} (216 Ma) and ε_{Nd} (216 Ma) values are inversely correlated in the conventional isotope diagram (Fig. 8), indicating that the magma evolution did not occur in a closed system and that continental contamination seems to have played a role more or less during the magma evolution, which is indicated by the binary diagrams of I_{Sr} (216 Ma) versus SiO_2 and ε_{Nd} (216 Ma) versus SiO_2 (Fig. 9a–b). Therefore, the unexpectedly high I_{Sr} ratio (0.712910) of sample KML1 seems to have resulted from upper crustal contamination, as the upper continental crust has an I_{Sr} ratio >0.7105 (Taylor and McLennan, 1985). As the contamination by the upper continental crust could not have changed the Nd isotopic composition, the values of the samples are similar to each other. The plot of La (ppm) versus the La/Yb ratio suggests that the partial melting was one of the important processes controlling the geochemical variations in the lamprophyres (Fig. 9d). In the plot of I_{Sr} (216 Ma) versus 1/Sr (Fig. 9c), the samples do not show a linear positive trend, which is inconsistent with a magma mixing process.

5.1.2. Source characteristics

The lamprophyre samples from the Gümüşhane region display a calc-alkaline geochemical signature, with low to moderate silica levels matching those of evolved melts derived from the mantle. The lamprophyre samples exhibit high concentrations of incompatible trace elements (LILE and LREE). In the N-MORB normalized multi-element diagram, there are significant negative Nb anomalies (Fig. 6a), suggesting that the lamprophyres were not derived from a normal MORB or OIB source. If they were derived from a normal MORB or OIB source, then positive Nb–Ti anomalies would be expected in the N-MORB-normalized trace element diagrams (e.g., Hofmann, 1997). All of the rocks are enriched in LREE, with almost similar REE abundances. Their Ce/Pb ratios (2–8) differ from those of oceanic basalts (~25; Hofmann, 1997), indicating that asthenospheric mantle melts were not likely the source. Sample KML10 is one of the most primitive lamprophyres investigated, as it is characterized by the highest MgO (8.90 wt.%), lowest SiO_2 (48.55 wt.%) and the most primitive isotopic compositions [I_{Sr} (216 Ma) = 0.706192, ε_{Nd} (216 Ma) = −1.4 and T_{DM} = 1.11; Table 3]. The previously reported geochemical and isotopic compositions of the sample, which are less radiogenic than that of depleted asthenospheric melt ($\varepsilon_{Nd}(t) = +5$; Basu et al., 1991), favor a source of enriched old subcontinental lithospheric mantle rather than a mafic lower crust for the lamprophyres. Their low Nb/La and La/Yb ratios are also consistent with those of lithospheric mantle (approximately <0.5) rather than OIB-like asthenospheric mantle melts (approximately >1; Bradshaw and Smith, 1994; Smith et al., 1999) (Fig. 10a). The Pb isotopic ratios resemble those of an EM2-type end-member (Fig. 8b, c), and their enrichment in LILEs and LREEs suggests an enriched lithospheric mantle as a source material. The calc-alkaline lamprophyre samples are characterized by a nearly flat HREE pattern. HREE fractionation in mafic lavas generally develops as a result of a melting of a mantle source that includes garnet or mantle enrichment by fluids/melts released from garnet-bearing subducted sediments (e.g., Avanzinelli et al., 2008; O'Neill, 1981). These indications suggest that garnet was not included in the mantle source of the rocks and that the melting occurred at shallower depths, indicating a spinel-bearing peridotite facies source.

The melting histories of the calc-alkaline lamprophyres are mirrored by the trace element modeling of Tb/Yb versus Ce/Yb ratios of the volcanic rocks (Fig. 10c). In this plot, a dynamic melting equation (Zou, 1998) is applied to an enriched depleted MORB mantle source composition (E-DMM; Workman and Hart, 2005) with spinel-lherzolite mineralogy (Kinzler, 1997). Nearly 1–7% partial melting of the E-DMM source may have produced the Tb/Yb versus Ce/Yb systematics of the samples. Garnet facies melting in the E-DMM source is also shown in Fig. 10c, creating higher Tb/Yb ratios in the melt with respect to those of spinel-facies melting. Alternatively, a spinel-facies partial melting model is also applied to the primitive mantle-normalized trace element amounts in the samples (Fig. 10d). The modeling results indicate that ~1–10% partial melting of the E-DMM source may explain the LREE and HREE levels in the samples. Such a melting model cannot explain the high LILE abundances and LILE enrichments over the HFSE ratios (negative Nb, Ta and Ti anomalies) of the samples. These relationships strongly suggest that the source of the calc-alkaline lamprophyres was

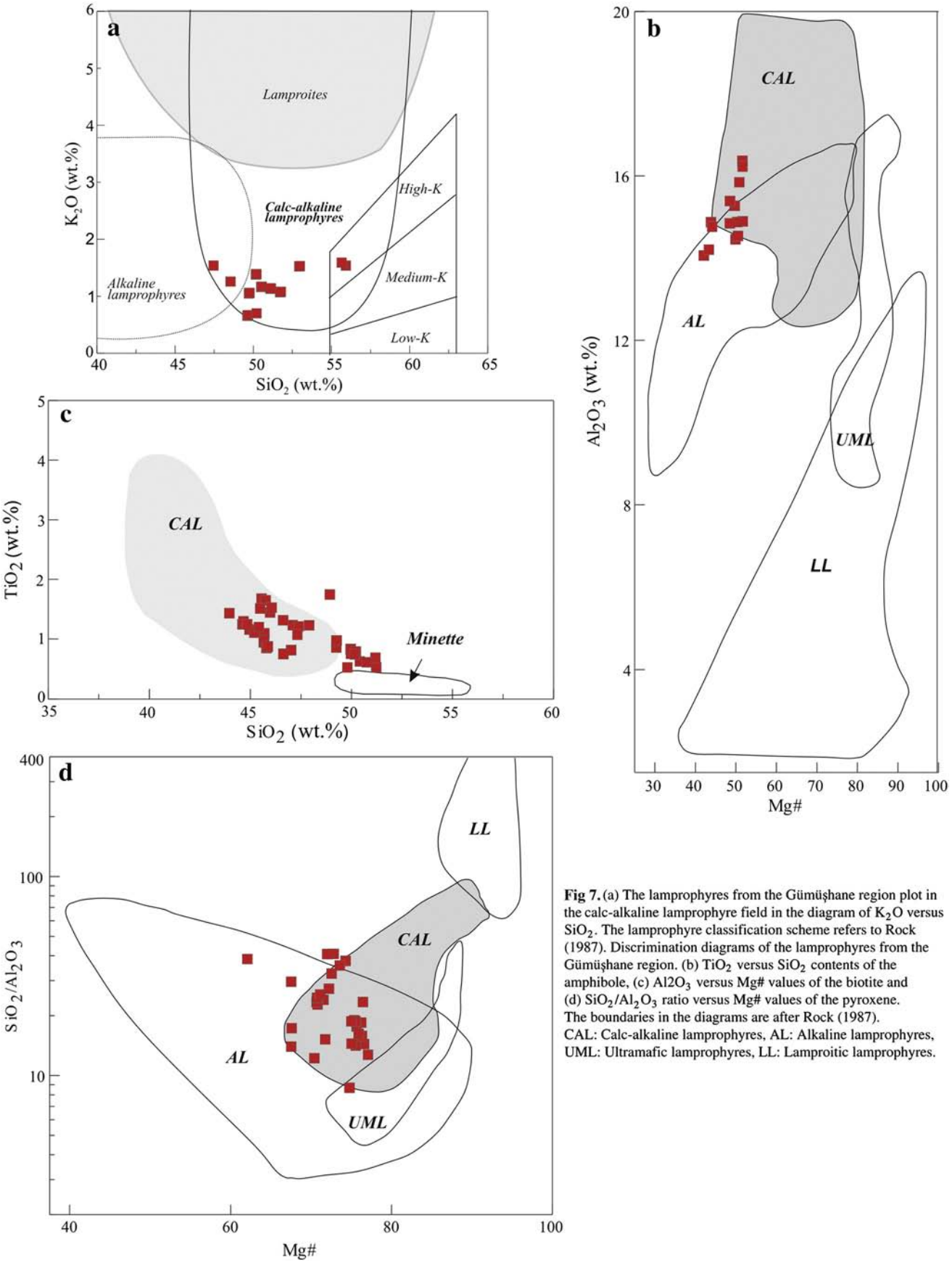

Fig 7. (a) The lamprophyres from the Gümüşhane region plot in the calc-alkaline lamprophyre field in the diagram of K_2O versus SiO_2. The lamprophyre classification scheme refers to Rock (1987). Discrimination diagrams of the lamprophyres from the Gümüşhane region. (b) TiO_2 versus SiO_2 contents of the amphibole, (c) $Al2O_3$ versus Mg# values of the biotite and (d) SiO_2/Al_2O_3 ratio versus Mg# values of the pyroxene. The boundaries in the diagrams are after Rock (1987). CAL: Calc-alkaline lamprophyres, AL: Alkaline lamprophyres, UML: Ultramafic lamprophyres, LL: Lamproitic lamprophyres.

Table 3
Whole-rock Sr and Nd isotopic compositions of the calc-alkaline lamprophyres from the Eastern Pontides.

Sample	[Rb] ppm	[Sr] ppm	$^{87}Rb/^{86}Sr$	$^{87}Sr/^{86}Sr$	2σ	I_{Sr} (216 Ma)	[Sm] ppm	[Nd] ppm	$^{147}Sm/^{144}Nd$	$^{143}Nd/^{144}Nd$	2σ	$\varepsilon_{Nd}(0)$	ε_{Nd} (216 Ma)	$f_{Sm/Nd}$	T_{DM} (Ga)
Calc-alkaline lamprophyres															
KML1	64.3	146.5	1.2728	0.713674	10	0.712910	2.84	10.3	0.1667	0.512669	9	0.6	0.8	−0.15	1.56
KML5	26.1	198.2	0.3819	0.708727	19	0.708500	3.56	12	0.1794	0.512773	8	2.6	2.7	−0.09	1.67
KML7	44.4	207.2	0.6214	0.708956	11	0.708595	4.3	14	0.1857	0.512759	10	2.4	2.4	−0.06	2.12
KML10	47.5	299.0	0.3443	0.706400	17	0.706192	2.28	7.7	0.1309	0.512547	6	−1.8	−1.4	−0.33	1.11
KML16	43.4	372.2	0.4156	0.707748	19	0.707512	3.68	18.1	0.1457	0.512848	8	4.1	4.1	−0.02	2.20

Note: $\varepsilon_{Nd} = (((^{143}Nd/^{144}Nd)_s/(^{143}Nd/^{144}Nd)_{CHUR} - 1) \times 10{,}000$, $f_{Sm/Nd} = (^{147}Sm/^{144}Sm)_s/(^{147}Sm/^{144}Sm)_{CHUR} - 1$, $(^{143}Nd/^{144}Nd)_{CHUR} = 0.512638$, and $(^{147}Sm/^{144}Sm)_{CHUR} = 0.1967$. The model ages were calculated using a linear isotopic ratio growth equation: $T_{DM} = 1/\lambda \times \ln(1 + ((^{143}Nd/^{144}Nd)_s - 0.51315)/((^{147}Sm/^{144}Nd)_s - 0.2137))$.

highly enriched, especially in LILEs, which can only be supplied by fluids or sediments derived from a subduction zone (Pearce, 1982; Pearce and Parkinson, 1993) metasomatizing the original mantle composition in the mantle wedge. Partial melting of such a mantle, affected by subduction zone processes, seems likely to have produced the trace element composition of the samples investigated.

5.1.3. Mantle enrichment

The enrichments in LILEs and LREEs with negative Nb and Ti anomalies are characteristic of subduction-related magmas and are commonly attributed to a mantle source that has been previously enriched in LILEs over HFSEs by the metasomatic activity of fluids derived from the subducted slab or sediments (e.g., Cameron et al., 2003; Elburg et al., 2002; Hawkesworth et al., 1997). The other possibility is the interaction between the lithospheric mantle and the volatile-rich material of the asthenosphere (Gibson et al., 1995; McKenzie, 1989). Such enrichment is usually an OIB-type signature, which is not consistent with the geochemical character of the calc-alkaline lamprophyres. Therefore, we propose that initial mantle enrichment was a plausible process in the development of the calc-alkaline lamprophyres investigated. The negative anomalies of Nb, Ta and Ti are typical of volcanic rocks formed in a subduction zone (Tatsumi and Kogiso, 1997). The regional geological data suggest that there is a consensus regarding the subduction of Paleotethyan oceanic slab in the region throughout the Triassic (Dokuz et al., 2010; Robertson and Dixon, 1984; Robinson et al., 1995; Tüysüz, 1999; Ustaömer and Robertson, 2010). Therefore, the calc-alkaline lamprophyres seem most likely to have been derived from the partial melting of an enriched mantle wedge in an active subduction setting at 216 Ma. We assume that the mantle enrichment occurred at great depth during the Triassic Period, when the Laurasian block was subducted beneath the Eastern Pontides. In such a case, a large amount of fluids and/or sediments triggered the metasomatization of the depleted mantle prior to its partial melting. However, the plot of U/Th versus Th/Nb for the samples suggest that the fluids coming from the subducted slab may have caused the enrichment (Fig. 10b). Beccaluva et al. (2004) suggest that an important feature of subduction-related mantle metasomatism is the formation of the hydrous mineral phase phlogopite or amphibole (or both). The element compatibility of phlogopite and amphibole can indicate which hydrous phase was formed in the lithospheric mantle source (Furman and Graham, 1999; Yang et al., 2004). The most primitive sample, KML10, has low Ba/Rb (4.57) and Nb/Th (1.23) ratios, whereas its Rb/Sr ratio (0.16) is relatively high, suggesting that the source contained phlogopite rather than amphibole. Spinel is depleted in REEs and Y, whereas garnet is enriched in HREEs and Y, and amphibole is enriched in MREEs. The melt is expected to be depleted in HREEs, with Y/Yb ratios >10 and (Ho/Yb)cn values >1.2 (Ge et al., 2002; Wu et al., 2002), if garnet was the major residue during melting. Lamprophyre sample KML10 from the area is depleted in HREEs, with Y/Yb = 10 and (Ho/Yb)cn = 1.04, suggesting that garnet was not the major residual phase, and spinel and/or amphibole were present in the residue. However, the relative enrichment in MREEs of the samples (Fig. 6b) indicates the instability of the amphibole in the residue after partial melting. Therefore, the enriched source material seems likely to have been a phlogopite-bearing spinel peridotite.

Table 4
Whole-rock lead isotopic composition of the calc-alkaline lamprophyres from the Eastern Pontides.

Sample	$^{206}Pb/^{204}Pb$	2σ	$^{207}Pb/^{204}Pb$	2σ	$^{208}Pb/^{204}Pb$	2σ
Calc-alkaline lamprophyres						
KML1	18.628	0.009	15.581	0.013	38.582	0.015
KLM5	18.458	0.014	15.602	0.018	38.451	0.019
KLM7	18.458	0.016	15.562	0.015	38.289	0.018
KML10	18.611	0.019	15.573	0.025	38.612	0.019
KML16	18.382	0.011	15.569	0.015	38.561	0.010

6. Geodynamic scenario for the calc-alkaline lamprophyre intrusions

The Late Triassic tectonothermal events in the Eastern Pontides are complex and still controversial, due to the limited extent of the plutonic rocks and their unknown geochemical fingerprints. Calc-alkaline and alkaline lamprophyres generally form in late- or post-orogenic settings (Allan and Carmichael, 1984; Chen and Zhai, 2003; Guo et al., 2004; Rock, 1991). The intrusion by lamprophyre in an active convergent margin of subduction character rarely occurs where the extensional stage is the dominant regime of the geodynamic system (Jackson et al., 1998; Luhr et al., 1989). In the investigated region, such back-arc extension was present throughout the Late Triassic (Dokuz, 2011; Okay et al., 1994; Robinson et al., 1995; Şengör and Yilmaz, 1981; Yilmaz et al., 1997). Hornblende $^{40}Ar/^{39}Ar$ dating of sample KML3 of the lamprophyres from the Karamustafa area (Gümüşhane) yielded a plateau age of 216.01 ± 10.64 Ma. The age data match the field observations of the lamprophyres emplaced in the Late Carboniferous granitoid rocks exposed in the Gümüşhane and Köse areas (Dokuz, 2011; Topuz et al., 2010). In addition, the obtained age data seem to be consistent with the timing of the back-arc related extension mentioned above. Indeed, the Late Triassic and Early Jurassic magmatic activities were very sporadic and small in volume compared to the Late Cretaceous magmatism in the region. Recently, Dokuz et al. (2010) suggested that the Early Jurassic Dutlupınar intrusion (ca. 188 Ma) formed in a back-arc extensional setting, whereas the Middle to Late Jurassic Sumbated intrusion (ca. 153 Ma) was identified as a collision or post-collision uplift type granitoid, based on its geochemical features. The southward subduction model (Dokuz et al., 2010; Şengör and Yilmaz, 1981; Şengör et al., 1984; Yilmaz et al., 1997) and northward subduction model (Robertson and Dixon, 1984; Robinson et al., 1995; Ustaömer and Robertson, 2010) have been proposed to explain the Late Triassic to Early Jurassic tectonomagmatic events in the region. According to the northward subduction model, the Pontides are thought of as a continental margin bordering the Paleotethys Ocean on the north. In contrast, in the southward subduction model, the Pontides are considered to have been the northern margin of Gondwana throughout Early Triassic to Early Jurassic times. In this model, Paleotethyan oceanic crust was subducted southward beneath Gondwana until Middle Jurassic time, and the Cimmerian continent, including the Pontides, was separated from Gondwana due to the subduction event in the Triassic. These events resulted in the opening of an intra-continental back-arc basin. Closure of the Paleotethyan Ocean led to an

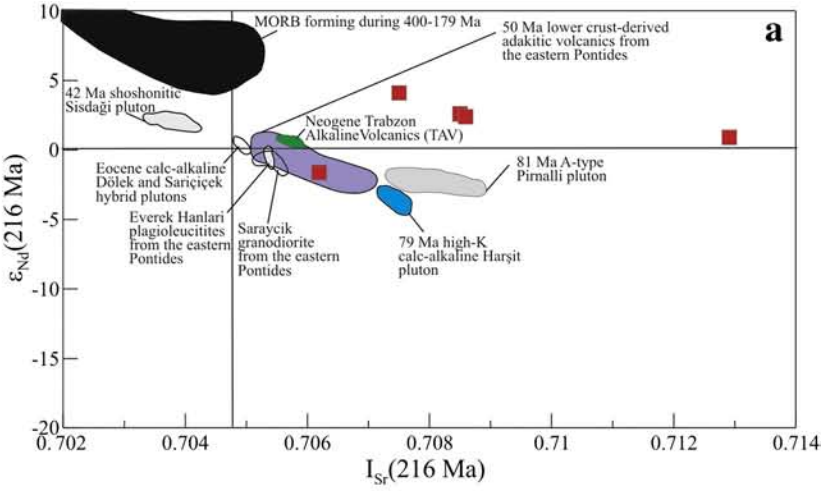
a
MORB forming during 400-179 Ma
50 Ma lower crust-derived adakitic volcanics from the eastern Pontides
42 Ma shoshonitic Sisdağı pluton
Neogene Trabzon Alkaline Volcanics (TAV)
Eocene calc-alkaline Dölek and Sariçiçek hybrid plutons
81 Ma A-type Pirnalli pluton
Everek Hanlari plagioleucitites from the eastern Pontides
Saraycik granodiorite from the eastern Pontides
79 Ma high-K calc-alkaline Harşit pluton
εNd(216 Ma)
ISr(216 Ma)

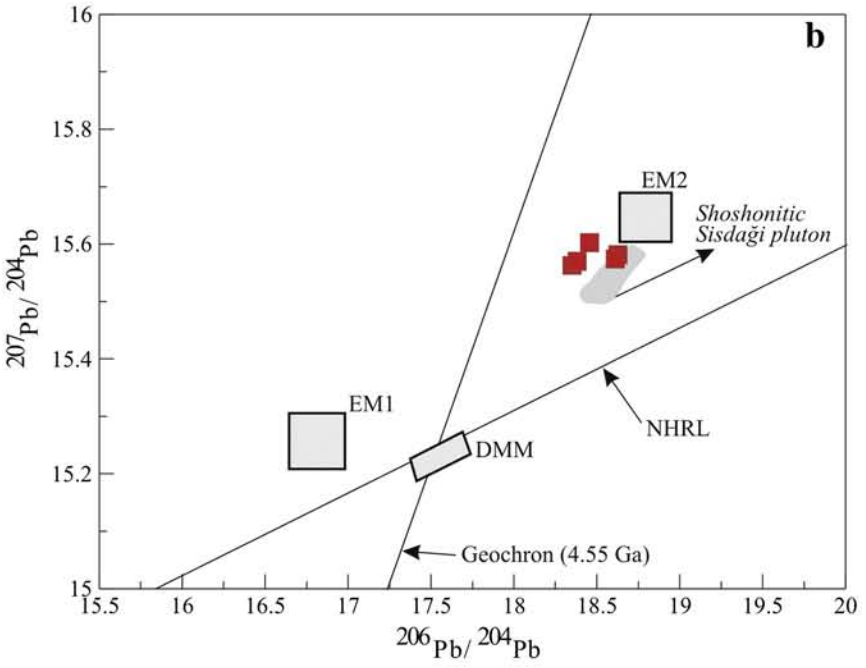
b
EM2
Shoshonitic Sisdağı pluton
EM1
DMM
NHRL
Geochron (4.55 Ga)
207Pb/204Pb
206Pb/204Pb

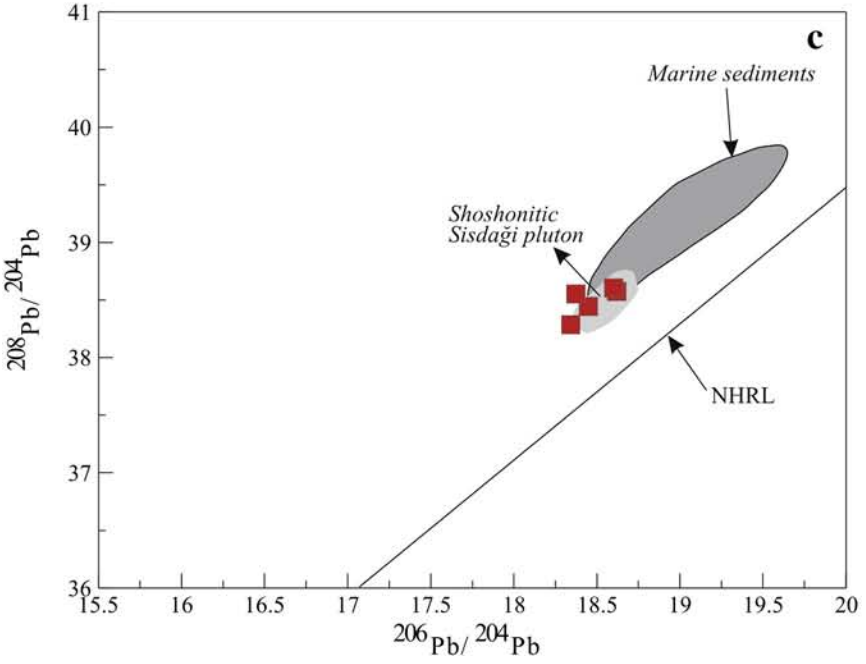
c
Marine sediments
Shoshonitic Sisdağı pluton
NHRL
208Pb/204Pb
206Pb/204Pb

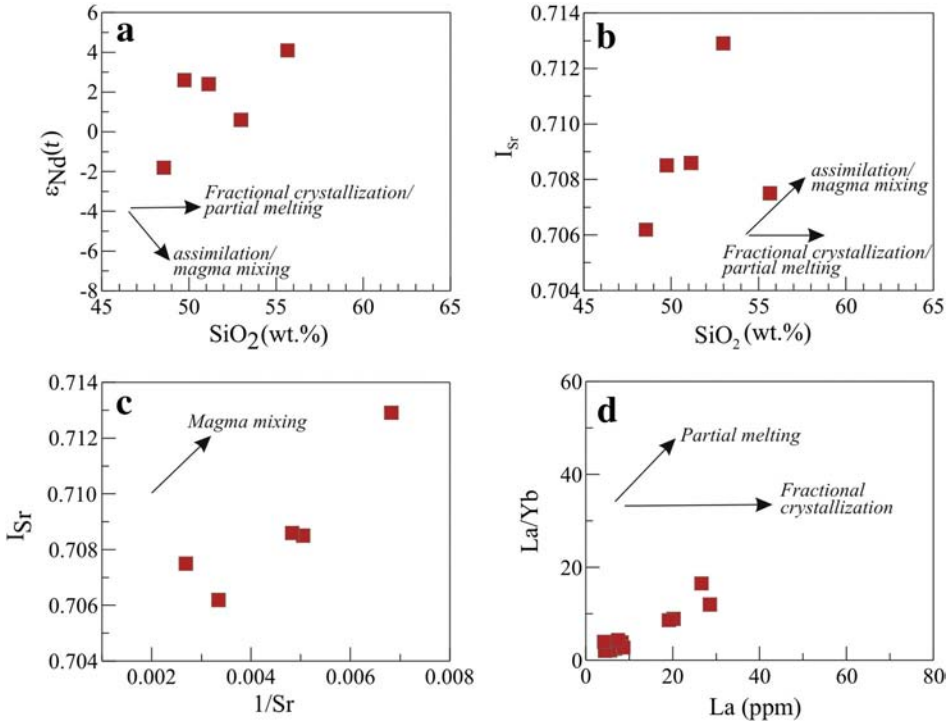

Fig. 9. Plots of (a) SiO_2 versus $\varepsilon_{Nd}(t)$; (b) SiO_2 versus I_{sr}; (c) 1/Sr versus I_{sr} and (d) La/Yb ratio versus La (ppm) content for the calc-alkaline lamprophyre studied.

amalgamation of the Pontides with the Laurasia during the Middle Jurassic (Dokuz et al., 2010; Şengör, 1979; Şengör and Yilmaz, 1981; Şengör et al., 1980, 1984; Yilmaz et al., 1997). Recent paleobiogeographical reconstructions based on the Early Jurassic brachiopod fauna from the Eastern Pontides indicate that the Cimmerian microcontinent was far from Gondwana and near the Eurasian margin of the Tethys, clearly supporting the southward subduction model in the Early Jurassic (Vörös and Kandemir, 2011). This geodynamic model is also consistent with the generation of the Early to Middle Jurassic magmatism in the Yusufeli region in the Eastern Pontides reported by Dokuz et al. (2010). For all of these reasons, the southward subduction of the Paleotethyan oceanic slab seems to be more consistent with the nature and geochemical fingerprints of the Late Triassic calc-alkaline lamprophyre intrusions. In the southward subduction model, it is thought that the northern margin of the Paleotethys Ocean was passive, and the subducted oceanic crust progressively become cold and older. This led to a steeper subduction angle, and trench roll-back occurred (Vlaar, 1989). Then, the over-riding continental plate was rapidly thinned by extension. The extensional events induced the upwelling of hot asthenospheric mantle, providing suitable conditions for the melting of an enriched subcontinental lithospheric mantle above the Paleotethyan oceanic slab.

A subduction-related setting for the calc-alkaline lamprophyres is mirrored by their enriched LILE and depleted HFSE compositions, which are indicative of not only subduction-related magmas but also post-collision related products. Based on the whole-rock and mineral chemistry data, the Eastern Pontides calc-alkaline lamprophyres, when plotted on the tectonic discrimination diagrams, might have originated in a subduction-related environment (Fig. 11a, b). Therefore, subduction-related back-arc extension rather than post-collisional extension seems likely to account for the genesis of the calc-alkaline lamprophyre intrusions in the region. The essential relationships between the petrogenesis of the calc-alkaline lamprophyres and the Late Triassic tectonic evolution of the Eastern Pontides may be summarized as follows: We suggest that the Late Triassic calc-alkaline lamprophyres formed in an extensional environment of a subduction setting. At 216 Ma, continental back-arc extension that was possibly related to slab roll-back induced the upwelling of asthenospheric mantle and caused a low degree (2 to 5%) of melting of previously enriched subcontinental lithospheric mantle composed of spinel-bearing lherzolite beneath the Pontides (Fig. 12). As a consequence of the mantle melting, scattered small volumes of Late Triassic to Early Jurassic intrusions, certain of which are calc-alkaline lamprophyres in composition, likely formed during a period of extension of the continental margin. Certain of these rocks are the calc-alkaline lamprophyre intrusions emplaced in an extensional environment of a subduction setting. Their distribution may reflect the transition from a compressional arc setting to an extensional setting at ~216 Ma in the Eastern Pontides.

7. Conclusions

The lamprophyres of the Eastern Pontides are characterized by a calc-alkaline and high-K calc-alkaline signature and an age of 216.01 ± 10.64 Ma. These rocks appear to be derived from an old subcontinental lithospheric mantle. The trace element modeling suggests that a low degree of partial melting (~1–10%) of an

Fig. 8. (a) Nd–Sr isotope compositions of the calc-alkaline lamprophyres from Gümüşhane region in the Eastern Pontides. Data sources are as follows: 400–179 Ma MORB are from Mahoney et al. (1998), Xu et al. (2003) and Tribuzio et al. (2004). 50 Ma Eastern Pontides adakitic lower crustal-derived volcanics, Eastern Pontides lower crustal-derived Saraycik granodiorite, Eastern Pontide Paleocene plagioleucitites, and high-K calc-alkaline Harşit rocks were taken after Karsli et al. (2010b), Topuz et al. (2005), Altherr et al. (2008) and Karsli et al. (2010a), respectively. Eocene Dölek and Sariçiçek hybrid plutons are after Karsli et al. (2007). The A-type plutons from the Eastern Pontides are from Karsli et al. (2012a). (b) Plots of (a) $^{207}Pb/^{204}Pb$ versus $^{206}Pb/^{204}Pb$ and (c) $^{208}Pb/^{204}Pb$ versus $^{206}Pb/^{204}Pb$ for the selected samples from the calc-alkaline lamprophyres. EM1 and EM2 were taken after Zindler and Hart (1986). The Northern Hemisphere Reference Line (NHRL) and Geochron (4.55 Ga) are also shown for comparison.

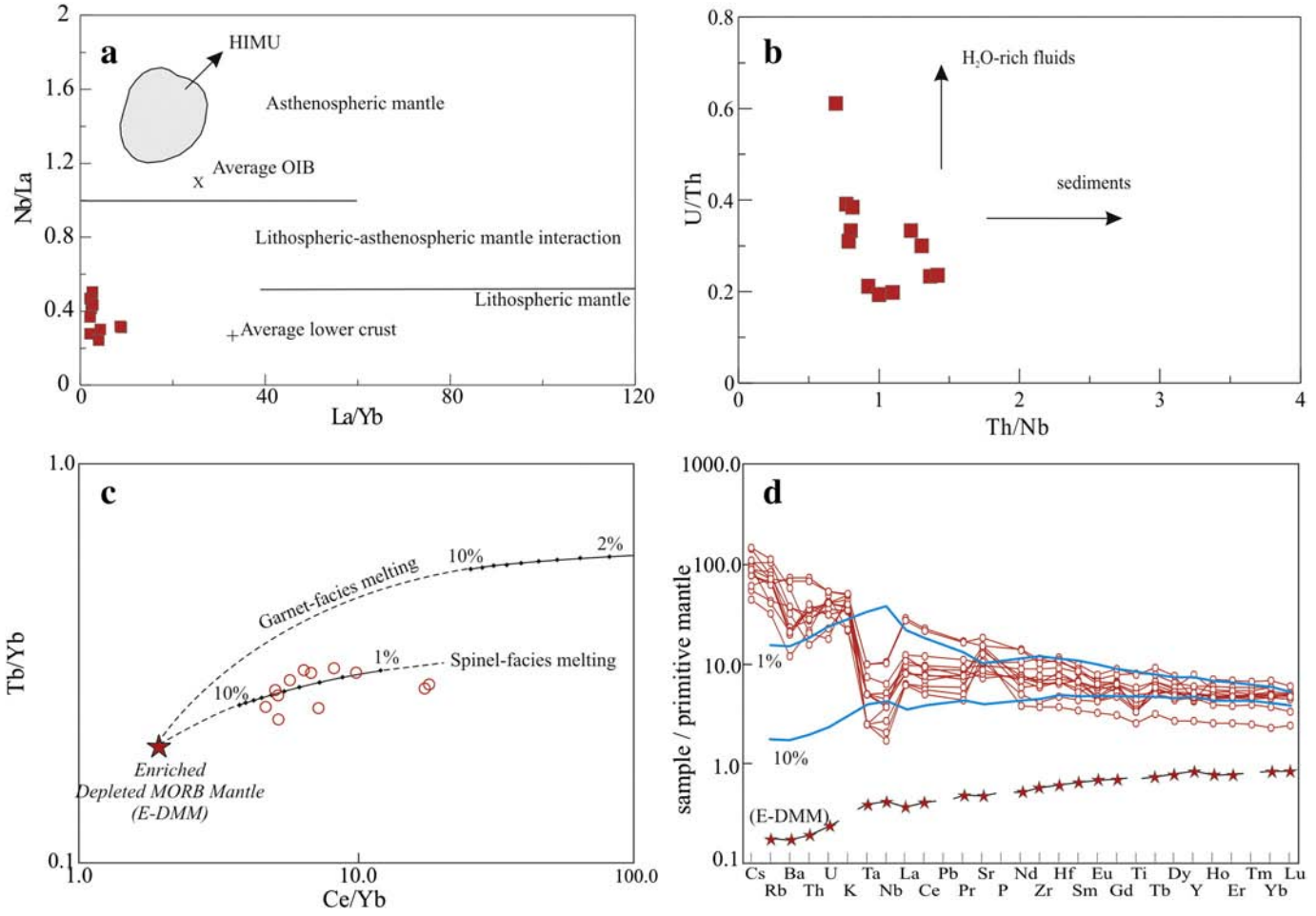

Fig. 10. (a) The Nb/La versus La/Yb variation diagram for the calc-alkaline lamprophyres from the Gümüşhane region in the Eastern Pontides. Average OIB is taken from Fitton et al. (1991) and average lower crust is after Chen and Arculus (1995). Dashed lines separating fields of the asthenospheric, lithospheric and mixed mantle, and the HIMU-OIB field are after Smith et al. (1999) and Weaver et al. (1987), respectively. (b) U/Th versus Th/Nb plot for the calc-alkaline lamprophyres from the Gümüşhane region. MORB is taken from Sun and McDonough (1989) and OIB is after Foley et al. (2002). (c) Partial melting models for the calc-alkaline lamprophyres from the Gümüşhane region in the Eastern Pontides (Tb/Yb vs Ce/Yb plot) and (d) Primitive mantle (PM)-normalized trace element patterns (PM normalizing values are from Palme and O'Neill (2004)). Melting curves were calculated by using closed-system non-modal dynamic melting equation (e.g., Zou, 1998) with PETROMODELER program of Ersoy (2013). Starting composition is enriched–depleted MORB mantle (E-DMM; Workman and Hart, 2005). The partition coefficients are compiled from McKenzie and O'Nions (1991), Green et al. (2000), and Adam and Green (2006). Garnet- and spinel-facies melting curves use mineral assemblages of $Ol_{0.60(0.03)} + Opx_{0.20(-0.16)} + Cpx_{0.10(0.88)} + Gt_{0.10(0.09)}$ (Walter, 1998) and $Ol_{0.53(-0.06)} + Opx_{0.27(0.28)} + Cpx_{0.17(0.67)} + Sp_{0.03(0.11)}$, respectively (Kinzler, 1997).

enriched, phlogopite-bearing spinel peridotite may have generated the unique composition of the calc-alkaline lamprophyres. Subsequently, the mafic parent magma ascended to its final chamber in the upper crust and underwent limited fractional crystallization and minor crustal contamination. The slab-derived fluids modified the old subcontinental lithospheric mantle. Upwelling of the asthenosphere triggered by back-arc extensional events in a subduction setting caused partial melting of the enriched mantle wedge. Back-arc extension due to southward subduction of the Paleotethys Ocean crust during the Late Triassic (at 216 Ma) is considered a plausible mechanism for the formation of the calc-alkaline lamprophyres in the Eastern Pontides, NE Turkey.

Supplementary data to this article can be found online at http://dx.doi.org/10.1016/j.lithos.2014.02.022.

Acknowledgments

We are most grateful to the staff of the Isotopic Laboratory of the Institute of Geology, Chinese Academy of Geological Sciences, in Beijing. This study was partly supported by the Scientific and Technological Research Council of Turkey (TÜBITAK) with grant # 108Y200. Special thanks go to E. Yalçin Ersoy for the geochemical modeling. Thanks are due to Andrew Kerr for his editorial handlings and two anonymous reviewers for their accurate and constructive reviews.

References

Adam, J., Green, T., 2006. Trace element partitioning between mica- and amphibole-bearing garnet lherzolite and hydrous basanitic melt: 1. Experimental results and the investigation of controls on partitioning behavior. Contributions to Mineralogy and Petrology 152, 1–17.

Allan, J.F., Carmichael, I.S.E., 1984. Lamprophyric lavas in the Colima graben, SW Mexico. Contributions to Mineralogy and Petrology 88, 203–216.

Altherr, R., Topuz, G., Siebel, W., Şen, C., Meyer, H.-P., Satır, M., 2008. Geochemical and Sr–Nd–Pb isotopic characteristics of Paleocene plagioleucitites from the Eastern Pontides (NE Turkey). Lithos 105, 149–161.

Arslan, M., Aslan, Z., 2006. Mineralogy, petrography and whole-rock geochemistry of the Tertiary granitic intrusions in the Eastern Pontides, Turkey. Journal of Asian Earth Sciences 27, 177–193.

Avanzinelli, R., Elliot, T., Tommasini, S., Conticelli, S., 2008. Constraints on the genesis of potassium-rich Italian volcanic rocks from U/Th disequilibrium. Journal of Petrology 49, 195–223.

Awdankiewicz, M., 2007. Late Paleozoic lamprophyres and associated mafic subvolcanic rocks of the Sudetes (SW Poland): petrology, geochemistry and petrogenesis. Geologia Sudetica 39, 11–97.

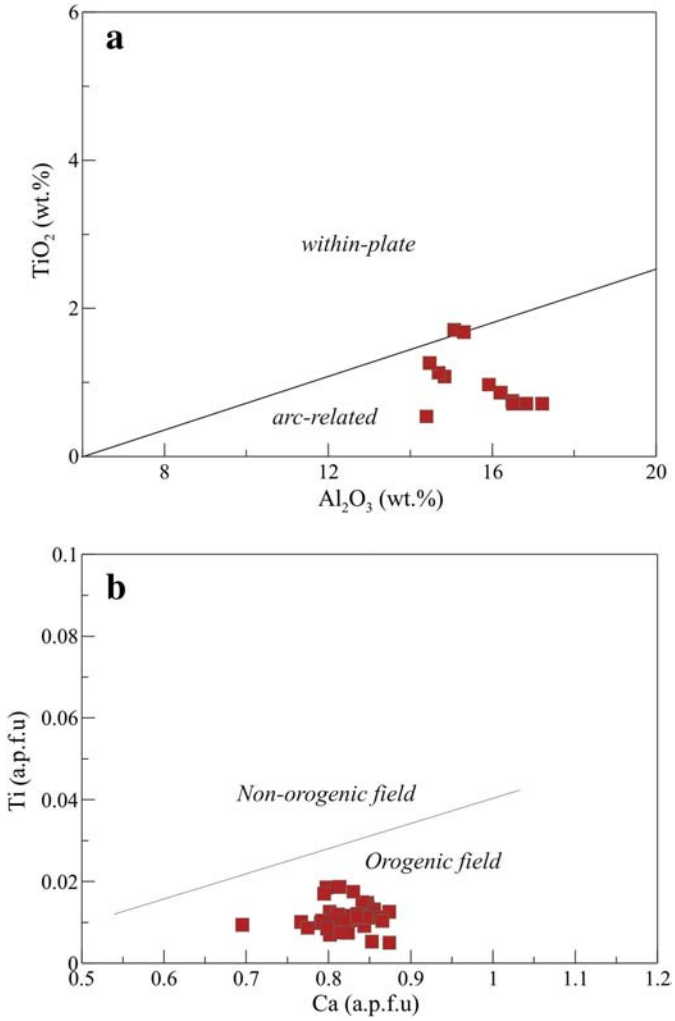

Fig. 11. Discrimination diagrams deciphering the tectonic setting for the calc-alkaline lamprophyres studied. (a) TiO_2 versus Al_2O_3 discrimination diagram for distinguishing within-plate and arc-related basalts (Muller et al., 1993). (b) Ti (a.p.f.u) versus Ca (a.p.f.u) diagram of clinopyroxene from the calc-alkaline lamprophyres.
The boundary was taken from Sun and Bertrad (1991).

Aydin, F., Şen, C., Sadiklar, M.B., 1997. Geological, mineralogical and geochemical characteristics of calc-alkaline lamprophyres in Paleozoic aged Gümüşhane Granitoid. Geosound 30, 613–624.

Aydin, F., Karsli, O., Chen, B., 2008. Petrogenesis of the Neogene alkaline volcanics with implications for post collisional lithospheric thinning of the Eastern Pontides, NE Turkey. Lithos 104, 249–266.

Aydin, F., Thompson, R., Karsli, O., Uchida, H., Burt, J.B., Downs, R.T., 2009. C2/c pyroxene phenocrysts from three potassic series in Neogene alkaline volcanics, Ne Turkey: their crystal chemistry with petrogenetic significance as an indicator of P–T conditions. Contributions to Mineralogy and Petrology 158, 131–147.

Aydinçakir, E., Şen, C., 2013. Petrogenesis of the post-collisional volcanic rocks from the Borçka (Artvin) area: implications for the evolution of the Eocene magmatism in the Eastern Pontides (NE Turkey). Lithos 172–173, 98–117.

Basu, A.R., Wang, J.W., Huang, W.K., Xie, G.H., Tatsumoto, M., 1991. Major element, REE, and Pb, Nd and Sr isotopic geochemistry of Cenozoic volcanic rocks of eastern China: implications for their origin from suboceanic-type mantle reservoirs. Earth and Planetary Science Letters 150, 149–169.

Beard, A.D., Downes, H., Vetrin, V., Kempton, P.D., Maluski, H., 1996. Petrogenesis of Devonian lamprophyre and carbonatite minor intrusions, Kandalaksha Gulf (Kola Peninsula, Russia). Lithos 39, 93–119.

Beccaluva, L., Bianchini, G., Bonadiman, C., Siena, F., Vaccaro, C., 2004. Coexisting anorogenic and subduction-related metasomatism in the mantle xenoliths from the Betic Cordillera (southern Spain). Lithos 75, 67–87.

Boynton, W.V., 1984. Cosmochemistry of the rare earth elements: meteorite studies. In: Henderson, P. (Ed.), Rare Earth Element Geochemistry. Elsevier, Amsterdam, pp. 63–114.

Boztuğ, D., Harlavan, Y., 2008. K–Ar ages of granitoids unravel the stages of Neo-tethyan convergence in the Eastern Pontides and central Anatolia, Turkey. International Journal of Earth Sciences 97, 585–599.

Boztuğ, D., Jonckheere, R., Wagner, G.A., Yeğingil, Z., 2004. Slow Senonian and fast Paleocene–Early Eocene uplift of the granitoids in the Central Eastern Pontides, Turkey: apatite fission-track results. Tectonophysics 382, 213–228.

Boztuğ, D., Erçin, A.I., Kuruçelik, M.K., Göç, D., Kömür, I., Iskenderoğlu, A., 2006. Geochemical characteristics of the composite Kackar batholith generated in a Neo-Tethyan convergence system, eastern Pontides, Turkey. Journal of Asian Earth Sciences 27, 286–302.

Bradshaw, T.K., Smith, E.I., 1994. Polygenetic Quaternary volcanism at Crater Flat, Nevada. Journal of Volcanology and Geothermal Research 63, 165–182.

Cameron, B.I., Walker, J.A., Carr, M.J., Patino, L.C., Matias, O., Feigenson, M.D., 2003. Flux versus decompression melting at stratovolcanoes in southeastern Guatemala. Journal of Volcanology Geothermal Research 119, 21–50.

Çapkınoğlu, Ş., 2003. First records of conodonts from the Permo-Carboniferous of Demirözü (Bayburt), Eastern Pontides, NE Turkey. Turkish Journal of Earth Sciences 12, 199–217.

Carlier, G., Lorand, J.P., Audebaud, E., Kienast, J.R., 1997. Petrology of unusual orthopyroxene-bearing minette suite from southeastern Peru, Eastern Andean Cordillera: Al-rich lamproites contaminated by peraluminous granites. Journal of Volcanology Geothermal Research 75, 59–87.

Chen, W., Arculus, R.J., 1995. Geochemical and isotopic characteristics of lower crustal xenoliths, San Francisco Volcanic Field, Arizona, U.S.A. Lithos 110, 99–119.

Chen, B., Zhai, M., 2003. Geochemistry of late Mesozoic lamprophyre dykes from the Taihang Mountains, north China, and implications for the sub-continental lithospheric mantle. Geological Magazine 140, 87–93.

Çinku, M.C., Ustaömer, T., Hirt, A.M., Hisarli, Z.M., Heler, F., Orbay, N., 2010. Southward migration of arc magmatism during latest Cretaceous associated with slab steepening,

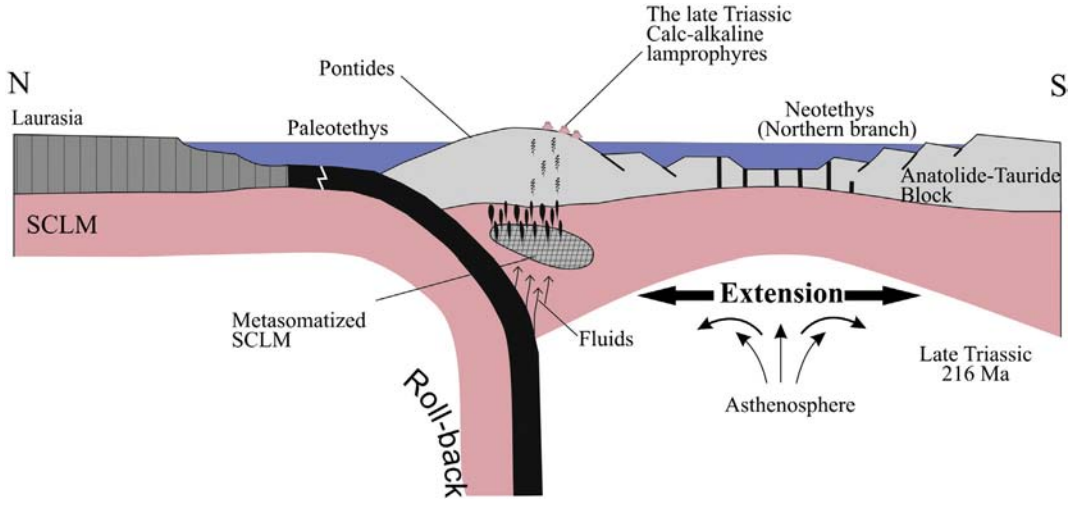

Fig. 12. A schematic illustration for the geodynamic environments of the Eastern Pontides during the Late Triassic to early Jurassic time. In the Late Triassic, continental back-arc extension possibly related to slab rollback induced upwelling of asthenospheric mantle, which is responsible for the partial fusion of an enriched mantle wedge.

East Pontides, N Turkey: new paleomagnetic data from the Amasya region. Physics of the Earth and Planetary Interiors 182, 18–29.
Currie, K.L., Williams, P.R., 1993. An Archean calc-alkaline lamprophyre suite, northeastern Yilgarn Block, western Australia. Lithos 31, 33–50.
Dokuz, A., 2011. A slab detachment and delamination model for the generation of Carboniferous high-potassium I-type magmatism in the Eastern Pontides, NE Turkey: Köse composite pluton. Gondwana Research 19, 926–944.
Dokuz, A., Tanyolu, E., 2006. Geochemical constraints on the provenance, mineral sorting and subaerial weathering of Lower Jurassic and Upper Cretaceous clastic rocks from the eastern Pontides, Yusufeli (Artvin), NE Turkey. Turkish Journal of Earth Sciences 15, 181–209.
Dokuz, A., Tanyolu, E., Genç, S., 2006. A mantle- and a lower crust-derived bimodal suite in the Yusufeli (Artvin) area, NE Turkey: trace element and REE evidence for subduction-related rift origin of Early Jurassic Demirkent intrusive complex. International Journal of Earth Sciences 95, 370–394.
Dokuz, A., Karsli, O., Chen, B., Uysal, I., 2010. Sources and petrogenesis of Jurassic granitoids in the Yusufeli area, Northeastern Turkey: implication for pre- and post-collisional lithospheric thinning of the Eastern Pontides. Tectonophysics 480, 259–279.
Dokuz, A., Uysal, İ., Kaliwoda, M., Karsli, O., Ottley, C.J., Kandemir, R., 2011. Early abyssal- and late SSZ-type vestiges of the Rheic oceanic mantle in the Variscan basement of the Sakarya Zone, NE Turkey: implications for the sense of subduction and opening of the Paleotethys. Lithos 127, 176–191.
Dokuz, A., Uysal, I., Siebel, W., Turan, M., Duncan, R., Akçay, M., 2013. Post-collisional adakitic volcanism in the eastern part of the Sakarya Zone, Turkey: evidence for slab and crustal melting. Contributions to Mineralogy and Petrology 166, 1443–1468.
Duggan, M.B., Jaques, A.L., 1996. Mineralogy and geochemistry of Proterozoic shoshonitic lamprophyres from the Tennant Creek Inlier, northern territory. Australian Journal of Earth Sciences 43, 269–278.
Elburg, M.A., Bergen, M.V., Hoogewerff, J., Foden, J., Vroon, P., Zulkarnain, I., Nasution, A., 2002. Geochemical trends across an arc–continent collision zone: magma sources and slab–wedge transfer processes below the Pantar Strait volcanoes, Indonesia. Geochimica et Cosmoschimica Acta 66, 2771–2789.
Ersoy, E.Y., 2013. PETROMODELER (Petrological Modeler): a Microsoft® Excel© spreadsheet program for modeling melting, mixing, crystallisation and assimilation processes in magmatic systems. Turkish Journal of Earth Science 22, 115–125.
Fitton, J.G., James, D., Leeman, W.P., 1991. Basic magmatism associated with Late Cenozoic extension in the western United States: compositional variations in space and time. Journal of Geophysical Research 96, 13693–13712.
Foley, S., Tiepolo, M., Vannucci, R., 2002. Growth of early continental crust controlled by melting of amphibolite in subduction zones. Nature 417, 837–840.
Frey, F.A., Green, E.H., Roy, S.D., 1978. Integrated model of basalt petrogenesis: a study of quartz toleiities to olivine melilites from southeastern Australia, utilizing geochemical experimental data. Journal of Petrology 19, 463–513.
Furman, T., Graham, D., 1999. Erosion of lithospheric mantle beneath the East African Rift system: geochemical evidence from the Kivu volcanic province. Lithos 48, 237–262.
Ge, X.Y., Li, X.H., Chen, Z.G., Li, W., 2002. Geochemistry and petrogenesis of Jurassic high Sr/low Y granitoids in the eastern China: constraints on crustal thickness. Chinese Sciences Bulletin 47, 962–968.
Gibson, S.A., Thompson, R.N., Leonardos, O.H., Dickin, A.P., Mithchell, J.G., 1995. The late Cretaceous impact of the Trindade mantle plume: evidence from large-volume, mafic, potassic magmatism in SE Brazil. Journal of Petrology 36, 189–229.
Görür, N., 1997. In: Robinson, A.G. (Ed.), Cretaceous Syn- to Post-rift Sedimentation on the Southern Continental Margin of the Western Black Sea Basin, pp. 227–240.
Green, T., Blundy, J.D., Adam, J., Yaxley, G.M., 2000. SIMS determination of trace element partition coefficients between garnet, clinopyroxene and hydrous basaltic liquids at 2–7.5 Gpa and 1080–1200 °C. Lithos 53, 165–187.
Gumbel Von, C.W., 1874. Die Palaeolithischen Eruptivegesteine des Fichtelgeberges. Franz, Munchen.
Guo, F., Fan, W., Wang, Y., Zhang, M., 2004. Origin of early Cretaceous calc-alkaline lamprophyres from the Sulu orogen in eastern China: implications for enrichment processes beneath continental collisional belt. Lithos 78, 291–305.
Hart, S., 1984. A large scale isotopic anomaly in the southern hemisphere mantle. Nature 47, 753–757.
Hawkesworth, C.J., Turner, S.P., McDermott, F., Peate, D.W., van Calsteren, P., 1997. U–Th isotopes in arc magmas: implications for element transfer from the subducted crust. Sciences 276, 551–555.
Hisarli, Z.M., 2011. Paleomagnetic constraints on the late Cretaceous and early Cenozoic tectonic history of the Eastern Pontides. Journal of Geodynamics 52, 114–128.
Hofmann, A.W., 1997. Mantle geochemistry: the message from oceanic volcanism. Nature 385, 219–229.
Jackson, T.A., Lewis, J.F., Scott, P.W., Manning, P.A.S., 1998. The petrology of lamprophyre dikes in the above rocks granitoid, Jamaica: evidence of rifting above a subduction zone during the early Tertiary. Caribbean Journal of Science 34, 1–11.
Kandemir, R., Lerosey-Aubril, R., 2011. First report a trilobite in the Carboniferous of Eastern Pontides, NE Turkey. Turkish Journal of Earth Sciences 20, 179–183.
Kandemir, R., Yilmaz, C., 2009. Lithostratigraphy, facies, and deposition environment of the lower Jurassic Ammonitico Rosso type sediments (ARTS) in the Gümüşhane area, NE Turkey: implications for the opening of the northern branch of the Neo-Tethys Ocean. Journal of Asian Earth Sciences 34, 586–598.
Karsli, O., Chen, B., Aydin, F., Şen, C., 2007. Geochemical and Sr–Nd–Pb isotopic compositions of the Eocene Dölek and Sariçiçek Plutons, Eastern Turkey: implications for magma interaction in the genesis of high-K calc-alkaline granitoids in a post-collision extensional setting. Lithos 98, 67–96.
Karsli, O., Dokuz, A., Uysal, I., Aydin, F., Bin, C., Kandemir, R., Wijbrans, R.J., 2010a. Relative contributions of crust and mantle to generation of Campanian high-K calc-alkaline I-type granitoids in a subduction setting, with special reference to the Harşit pluton, Eastern Turkey. Contributions to Mineralogy and Petrology 160, 467–487.
Karsli, O., Dokuz, A., Uysal, I., Aydin, F., Kandemir, R., Wijbrans, R.J., 2010b. Generation of the Early Cenozoic adakitic volcanism by partial melting of mafic lower crust, Eastern Turkey: implications for crustal thickening to delamination. Lithos 114, 109–120.
Karsli, O., Uysal, I., Ketenci, M., Dokuz, A., Aydin, F., Kandemir, R., Wijbrans, J., 2011. Adakite-like granitoid porphyries in Eastern Pontides, NE Turkey: potential parental melts and geodynamic implications. Lithos 127, 354–372.
Karsli, O., Caran, Ş., Dokuz, A., Çoban, H., Bin, C., Kandemir, R., 2012a. A-type granitoids from the Eastern Pontides, NE Turkey: records for generation of hybrid A-type rocks in a subduction-related environment. Tectonophysics 530–531, 208–224.
Karsli, O., Dokuz, A., Uysal, I., Ketenci, M., Chen, B., Kandemir, R., 2012b. Deciphering the shoshonitic monzonites with I-type characteristic, the Sisdağı pluton, NE Turkey: magmatic response to continental lithospheric thinning. Journal of Asian Earth Science 51, 45–62.
Kaygusuz, A., Siebel, W., Şen, C., Satir, M., 2008. Petrochemistry and petrology of I-type granitoids in an arc setting: the composite Torul pluton, Eastern Pontides, NE Turkey. International Journal of Earth Sciences 97, 739–764.
Kinzler, R.J., 1997. Melting of mantle peridotite at pressures approaching the spinel to garnet transition: application to midocean ridge basalt petrogenesis. Journal of Geophysical Research 102, 853–874.
Koçyiğit, A., Altiner, D., 2002. Tectonostratigraphic evolution of the North Anatolian Paleorift (NAPR): Hettangian–Aptian passive continental margin of the Northern Neo-Tethys, Turkey. Turkish Journal of Earth Sciences 11, 169–191.
Le Bas, M.J., Le Maitre, R.W., Streckeisen, A., Zanetti, B., 1986. A chemical classification of volcanic rocks based on the total alkali–silica diagram. Journal of Petrology 27, 745–750.
Le Maitre, R.W., 1989. A Classification of Igneous Rocks and Glossary of Terms (Recommendations of the International Union of Geological Sciences Sub-commission on the Systematics of Igneous Rocks). Blackwell, Oxford (193 pp.).
Leake, E.B., 21 collaborators, 1997. Nomenclature of amphiboles: report of the subcommittee on amphiboles of the International Mineralogical Association Commission on new minerals and mineral names. European Journal of Mineralogy 9, 623–651.
Luhr, J.F., Allan, J.F., Carmichael, I.S.E., Nelson, S.A., Hasenaka, T., 1989. Primitive calc-alkaline and alkaline rock types from the western Mexican Volcanic Belt. Journal of Geophysical Research 94, 4515–4530.
Mahoney, J.J., Frei, R., Tejada, M.L.G., Mo, X.X., Leat, P.T., Nagler, T.P., 1998. Tracing the Indian Ocean mantle domain through time: isotopic results from old west Indian, east Tethyan and South Pacific seafloor. Journal of Petrology 39, 1285–1306.
McKenzie, D.P., 1989. Some remarks on the movement of small melt fractions in the mantle. Earth and Planetary Science Letters 95, 53–72.
McKenzie, D., O'Nions, R.K., 1991. Partial melt distributions from inversion of rare earth element concentrations. Journal of Petrology 32, 1021–1091.
Morimoto, N., Fabries, J., Ferguson, A.K., Ginzburg, I.V., Ross, M., Seifert, F.A., Zussman, J., Aoki, K., Gottardi, G., 1988. Nomenclature of pyroxenes. American Mineralogist 73, 1123–1133.
Müller, D., Groves, D.I., 1995. Potassic Igneous Rocks and Associated Gold–Copper Mineralization. Springer-Verlag 1–210.
Muller, D., Morris, B.J., Ferrand, M.J., 1993. Potassic alkaline lamprophyres with affinities to lamproites from the Karinya Syncline, South Australia. Lithos 30, 123–137.
Nédli, Z., Tóth, T.M., 2007. Origin and geodynamic significance of Upper Cretaceous lamprophyres from the Villány Mts (S Hungary). Mineralogy and Petrology 90, 73–107.
O'Neill, H.S.C., 1981. The transition between spinel lherzolite and garnet lherzolite, and its use as a Geobarometer. Contributions to Mineralogy and Petrology 77, 185–194.
Okay, A.I., Göncüoğlu, M.C., 2004. The Karakaya complex: a review of data and concepts. Turkish Journal of Earth Sciences 13 (2), 77–95.
Okay, A.I., Leven, E.J., 1996. Stratigraphy and paleontology of the upper Paleozoic sequences in the Pulur (Bayburt) region, Eastern Pontides. Turkish Journal of Earth Sciences 5, 145–155.
Okay, A.I., Şahintürk, Ö., 1997. Geology of the Eastern Pontides. In: Robinson, A.G. (Ed.), Regional and Petroleum Geology of the Black Sea and Surrounding Region. AAPG Memoir, 68, pp. 292–311.
Okay, A.I., Tüysüz, O., 1999. Tethyan sutures of northern Turkey. In: Durand, B., Jolivet, L., Horvath, F., Seranne, M. (Eds.), The Mediterranean Basins: Tertiary Extension Within the Alpine Orogen. Geological Society, London, Special Publication, 156, pp. 475–515.
Okay, A.I., Şengör, A.M.C., Görür, N., 1994. Kinematic history of the opening of the Black Sea and its effect on the surrounding regions. Geology 22, 267–270.
Okay, A.I., Monod, O., Monie, P., 2002. Triassic blueschists and eclogites from northwest Turkey: vestiges of the Paleo-Tethyan subduction. Lithos 64 (3–4), 155–178.
Palme, H., O'Neill, H.S.C., 2004. Cosmochemical estimates of mantle composition. In: Holland, H.D., Turekian, K.K. (Eds.), Treatise on Geochemistry, 2. Elsevier, Amsterdam, pp. 1–38.
Pearce, J.A., 1982. Trace element characteristics of lavas from destructive plate boundaries. In: Thorpe, R.S. (Ed.), Andesites. John Wiley and Sons, pp. 526–548.
Pearce, J.A., Parkinson, I.J., 1993. Trace element models for mantle melting: application to volcanic arc petrogenesis. In: Prichard, H.M., Alabaster, T., Harris, N.B., Neary, C.R. (Eds.), Magmatic Processes and Plate Tectonics. Geological Society of London, Special Publications, 76, pp. 373–403.
Peccerillo, A., Taylor, S.R., 1976. Geochemistry of Eocene calc-alkaline volcanic rocks from Kastamonu area, northern Turkey. Contributions to Mineralogy and Petrology 58, 63–81.
Pouchou, J.L., Pichoir, F., 1985. "PAP" (ø,ρ,Z) correction procedure for improved quantitative microanalysis. In: Armstrong, J.T. (Ed.), Microbeam analysis. San Francisco Press, pp. 104–106.

Prelevic, D., Foley, S.F., Romer, R.L., Cvetkovic, V., Downes, H., 2005. Tertiary ultrapotassic volcanism in Serbia: constraints on petrogenesis and mantle source characteristics. Journal of Petrology 46, 1443–1487.
Qiao, G., 1988. Normalization of isotopic dilution analyses—a new program for isotope mass spectrometric analysis. Scientica Sinica 31, 1263–1268.
Queen, M., Heaman, L.M., Hanes, J.A., Archibald, D.A., Farrar, E., 1996. $^{40}Ar/^{39}Ar$ phlogopite and U–Pb perovskite dating of lamprophyre dykes from the eastern Lake Superior region: evidence for a 1.14 Ga magmatic precursor to Midcontinent Rift volcanism. Canadian Journal of Earth Sciences 33, 958–965.
Robertson, A.H.F., Dixon, J.E., 1984. Introduction: aspects of the geological evolution of the eastern Mediterranean. In: Dixon, J.E., Robertson, A.H.F. (Eds.), The Geological Evolution of the Eastern Mediterranean. Geological Society London Special Publication, 17, pp. 1–74.
Robinson, A.G., Banks, C.J., Rutherford, M.M., Hirst, J.P.P., 1995. Stratigraphic and structural development of the Eastern Pontides, Turkey. Journal of Geological Society London 152, 861–872.
Rock, N.M.S., 1987. The nature and origin of lamprophyres: an overview. In: Fitton, J.G., Upton, B.G.J. (Eds.), Alkaline Igneous Rocks. Geological Society Special publications, 30, pp. 191–226.
Rock, N.M.S., 1991. Lamprophyres. Blackie and Son, Glasgow (225 pp.).
Rolland, Y., Perincek, D., Kaymakci, N., Sosson, M., Barrier, E., Avagyan, A., 2012. Evidence for ~80–75 Ma subduction jump during Anatolia–Tauride–Armenian block accretion and ~48 Ma Arabia–Eurasia collision in Lesser Caucasus–East Anatolia. Journal of Geodynamics 56–57, 76–85.
Şen, C., 2007. Jurassic volcanism in the Eastern Pontides: is it rift related or subduction related? Turkish Journal of Earth Sciences 16, 523–539.
Şengör, A.M.C., 1979. Mid-Mesozoic closure of Permo-Triassic Tethys and its implications. Nature 279, 590–593.
Şengör, A.M.C., Yilmaz, Y., 1981. Tethyan evolution of Turkey: a plate tectonic approach. Tectonophysics 75, 181–241.
Şengör, A.M.C., Yılmaz, Y., Ketin, İ., 1980. Remnants of Pre-Late Jurassic ocean in northern Turkey: fragments of Permian–Triassic Paleo-Tethys. Geological Society of America Bulletin 91, 599–609.
Şengör, A.M.C., Yılmaz, Y., Sungurlu, O., 1984. Tectonics of Mediterranean Cimmerides: nature and evolution of the western termination of Paleotethys. In: Dixon, J.E., Robertson, A.H.F. (Eds.), The Geological Evolution of the Eastern Mediterranean. Geological Society London, Special Publications, 17, pp. 77–112.
Şengör, A.M.C., Özeren, S., Genç, T., Zor, E., 2003. East Anatolian high plateau as a mantle-supported, north–south shortened domal structure. Geophysical Research Letters 30 (24), 8045. http://dx.doi.org/10.1029/2003GL017858.
Smith, E.I., Sánchez, A., Walker, J.D., Wang, K., 1999. Geochemistry of mafic magmas in the Hurricane volcanic field, Utah: implications for small- and large-scale chemical variability of the lithospheric mantle. Journal of Geology 107, 433–448.
Srivastava, R.K., Chalapathi Rao, N.V., 2007. Petrology, geochemistry and tectonic significance of Paleoproterozoic alkaline lamprophyres from the Jungel Valley, Mahakoshal supracrustal belt, Central India. Mineralogy and Petrology 89, 189–215.
Sun, C.M., Bertrad, J., 1991. Geochemistry of clinopyroxenes in plutonic and volcanic sequences from the Yanbian Proterozoic ophiolites (Sichuan Province, China): petrogenetic and geotectonic implications. Schweizer Minealogische und Petrographische Mitteilungen 71, 243–259.
Sun, S.S., McDonough, W.E., 1989. Chemical and isotopic systematics of oceanic basalts: implications for mantle composition and processes. In: Saunders, A.D., Norry, M.J. (Eds.), Magmatism in the Ocean Basins. Special Publication. Geological Society of London, pp. 313–345.
Tappe, S., Foley, S.F., Jenner, G.A., Heaman, L.M., Kjarsgaard, B.A., Romer, R.L., Stracke, A., Joyce, N., Hoefs, J., 2006. Genesis of ultramafic lamprophyres and carbonatites at Aillik bay, Labrador: a consequence of incipient lithospheric thinning beneath the North Atlantic craton. Journal of Petrology 47, 1261–1315.
Tatsumi, Y., Kogiso, T., 1997. Trace element transport during dehydration processes in the subducted oceanic crust: 2. Origin of chemical and physical characteristics in arc magmatism. Earth and Planetary Science Letters 148, 207–210.
Taylor, S.R., McLennan, S.M., 1985. The continental crust: Its composition and evolution. Blackwell, Oxford pp. 73–93.
Topuz, G., Altherr, R., Schwarz, W.H., Siebel, W., Satir, M., Dokuz, A., 2005. Post-collisional plutonism with adakite-like signatures: the Eocene Saraycik granodiorite (Eastern Pontides, Turkey). Contributions to Mineralogy and Petrology 150, 441–455.
Topuz, G., Altherr, R., Schwarz, W.H., Dokuz, A., Meyer, H.P., 2007. Variscan amphibolite-facies rocks from the Kurtoğlu metamorphic complex. Gümüşhane area, Eastern Pontides, Turkey. International Journal of Earth Sciences 96, 861–873.
Topuz, G., Altherr, R., Wolfgang, S., Schwarz, W.H., Zack, T., Hasözbek, A., Mathias, B., Satir, M., Şen, C., 2010. Carboniferous high-potassium I-type granitoid magmatism in the Eastern Pontides: the Gümüşhane pluton (NE Turkey). Lithos 116, 92–110.
Topuz, G., Okay, A.I., Altherr, R., Schwarz, W.H., Siebel, W., Zack, T., Satir, M., Şen, C., 2011. Post-collisional adakite-like magmatism in the Ağvanis massif and implications for the evolution of the Eocene magmatism in the Eastern Pontides (NE Turkey). Lithos 125, 131–150.
Tribuzio, R., Thirlwall, M.F., Vannucci, R., Matthew, F., 2004. Origin of the gabbro–peridotite association from the Northern Apennine Ophiolites (Italy). Journal of Petrology 45, 1109–1124.
Tüysüz, O., 1999. Geology of the Cretaceous sedimentary basins of the Western Pontides. Geological Journal 34, 75–93.
Ustaömer, T., Robertson, H.F.A., 2010. Late Paleozoic–Early Cenozoic tectonic development of the Eastern Pontides (Artvin area), Turkey: stages of closure of Tethys along the southern margin of Eurasia. Special Publications, Geological Society London 340, 281–327.
Vlaar, N.J., 1989. Subduction of young lithosphere: lithospheric doubling, a possible scenario. In: Hart, S.R., Gulen, L. (Eds.), Crust/Mantle Recycling at Convergence Zone Dordrecht, Kluer, pp. 65–74.
Vörös, A., Kandemir, R., 2011. A new early Jurassic brachiopod fauna from the Eastern Pontides (Turkey). Neues Jahrbuch für Geologie und Paläontologie Abhandlungen 260, 343–363.
Walter, M.J., 1998. Melting of garnet peridotite and the origin of komatiite and depleted lithosphere. Journal of Petrology 39, 29–60.
Weaver, B.L., Wood, D.A., Tarney, J., Joron, J., 1987. Geochemistry of ocean island basalt from the South Atlantic: Ascension, Bouvet, St. Helena, Gough and Tristan da Cunha. In: Fitton, J.G., Upton, B.G.J. (Eds.), Alkaline Igneous Rocks. Journal of the Geological Society London, Special Publication no 30, pp. 253–267.
Wijbrans, J.R., Pringle, M.S., Koppers, A.A.P., Scheveers, R., 1995. Argon geochronology of small samples using the Vulcaan argon laser probe. Processes of Kon Ned Akad V Wetensh 98, 185–218.
Workman, R.K., Hart, S.R., 2005. Major and trace element composition of the depleted MORB mantle (DMM). Earth and Planetary Science Letters 231, 53–72.
Wu, F.Y., Ge, W.C., Sun, D.Y., 2002. The definition, discrimination of adakites and their geological role. In: Xiao, Q.H., Deng, J.F., Ma, D.Q. (Eds.), The Ways of Investigation on Granitoids (in China), Beijing. Geological Publishing House, pp. 172–191.
Xu, J.F., Castillo, P.R., Chen, F.R., Niu, H.C., Yu, X.Y., Zhen, Z.P., 2003. Geochemistry of late Paleozoic mafic igneous rocks from the Kuerti area, Xinjiang, northwest China: implications for backarc mantle evolution. Chemical Geology 193, 137–154.
Yang, J.H., Chung, S.I., Zhai, M.G., Zhou, X.H., 2004. Geochemical and Sr–Nd–Pb isotopic compositions of mafic dykes from the Jiaodong peninsula, China: evidence for vein-plus-peridotite melting in the lithospheric mantle. Lithos 73, 145–160.
Yilmaz, Y., 1972. Petrology and Structure of the Gümüşhane Granite and the Surrounding Rocks. NE Anatolia. (PhD Thesis) University College London, England (248 pp.).
Yilmaz, Y., Tüysüz, O., Yiğitbaş, E., Genç, Ş.C., Şengör, A.M.C., 1997. Geology and tectonic evolution of the Pontides. In: Robinson, A.G. (Ed.), Regional and Petroleum Geology of the Black Sea and Surrounding Region. Am. Assoc. Petrol. Geol. Mem, 68, pp. 183–226.
Zindler, A., Hart, S.R., 1986. Chemical geodynamics. Annual Review Earth Planetary Science 14, 493–571.
Zou, H.B., 1998. Trace element fractionation during modal and nonmodal dynamic melting and open-system melting: a mathematical treatment. Geochimica et Cosmochimica Acta 62, 1937–1945.